Overcoming barriers to T cell activation, infiltration and function in tumors

Melssen, M.M.

Citation

Melssen, M. M. (2021, January 26). *Overcoming barriers to T cell activation, infiltration and function in tumors*. Retrieved from https://hdl.handle.net/1887/139165

Cover Page

The handle http://hdl.handle.net/1887/139165 holds various files of this Leiden University dissertation.

Author: Melssen, M.M.
Title: Overcoming barriers to T cell activation, infiltration and function in tumors
Issue date: 2021-01-26

Chapter 6

Differential expression of CD49a and CD49b determines localization and function of tumor infiltrating CD8 T-cells

Marit M. Melssen, Robin S. Lindsay, Katarzyna Stasiak, Anthony B. Rodriguez, Amanda M. Briegel, Salwador Cyranowski, Melanie Rutkowski, Mark R. Conaway, Cornelis J.M. Melief, Sjoerd H. van der Burg, Ukpong Eyo, Craig L. Slingluff, Jr and Victor H. Engelhar

ABSTRACT

CD8 T-cell infiltration and effector activity in solid tumors are correlated with better overall survival of patients suggesting that the ability of T-cells to enter and to remain in contact with tumor cells supports tumor control. CD8 T-cells are known to express the collagen-binding integrins CD49a and CD49b, although little is known about the function of these integrins or how their expression is regulated in the tumor microenvironment (TME). Here, we found that tumor-infiltrating CD8 T-cells initially express CD49b, gain CD49a, and then lose the expression of CD49b over the course of tumor outgrowth. This differentiation sequence is driven by antigen-independent elements in the TME, although T-cell receptor stimulation further increased CD49a expression. On intratumoral CD49a-expressing CD8 T-cells, CD69 was upregulated in the absence of T-cell receptor signaling, consistent with both the establishment of a tissue resident memory-like T-cell phenotype, and a lack of productive antigen engagement. Imaging T-cells in live tumor slices revealed that CD49a increases their motility, especially of those in close proximity to tumor cells. Thus, CD49a may block the interaction of T-cells with tumor cells by not allowing productive engagement. Together, our results illuminate a new mechanism of CD8 T-cell dysfunction in tumors, which is driven by and dependent upon antigen-independent elements in the TME.

INTRODUCTION

Survival of cancer patients is prolonged in those whose tumors are robustly infiltrated by T-cells (1–3). The extent of T-cell representation in tumors depends on several factors (4), including their capacity to utilize homing mechanisms as well as their ability to survive and to be retained in the tumor microenvironment (TME). Homing mechanisms used by tumor-infiltrating T-cells depend on expression of homing receptor ligands VCAM-1, ICAM-1, E-selectin, and CXCR3-binding chemokines on tumor-associated vasculature (5–7). However, the processes of T-cell retention and localization in tumors are less well-studied and likely depend on antigen recognition, interaction with extracellular matrix (ECM) proteins, and expression of molecules that mediate tissue egress into lymphatics (8–15). Specifically, interaction with ECM could either retain T-cells in tumor tissue generally or sequester T-cells in ECM-rich areas, preventing them from engaging with tumor cells (16,17). T-cell interactions with ECM proteins, including collagens, can be mediated by integrins such as a1b1 (CD49a) and a2b1 (CD49b) (18). CD49a and CD49b predominantly bind to collagen type IV and type I, respectively (5,18–21). Blocking CD49a interaction with collagen *in vivo* has been shown to decrease the number of intraepithelial CD8 T-cells in the gut under homeostatic conditions and to decrease total T-cell numbers in mucosal tumors (22,23). Furthermore, CD49a signaling is associated with increased T-cell motility in tissues (24–26). Together, these findings suggest that interactions between ECM collagens and T-cell integrins in tumors could determine overall T-cell numbers and localization, and also their ability to engage with target cells productively. Importantly, whether these processes are supported or impaired by CD49a and CD49b equally and how each specifically impacts T-cell function in tumors remains to be elucidated.

CD49b is expressed on a fraction of effector T-cells in the context of arthritis, influenza or LCMV infection and in tumors, while CD49a expression is limited to a fraction of effector cells specifically localized to peripheral tissue sites in these models (18,21,27,28). CD49a is also expressed on tissue resident memory T-cells (T_{RM}) in lung, skin and mucosal sites (29). Neither CD49a or CD49b are expressed on naïve or circulating memory T-cells (18,30,31). T-cell receptor (TCR)-mediated activation is thus likely required for the expression of these integrins, while CD49a may additionally require stimulation provided by an element in the peripheral tissue microenvironment. We previously observed increased expression of CD49a and CD49b on human CD8 T cells after *in vitro* TCR stimulation, and expression was further enhanced by TGFβ, TNFα, and IL-2 (31). Others have found that the presence of CD49a$^+$ T_{RM} cells in mice depends on TGFβ and Notch signaling (32,33). However, it is not known whether any of these are dominant mediators of CD49a and CD49b expression during an immune response *in vivo*, or in chronic inflammatory environments or tumors. Thus, in addition to understanding their direct role in T-cell function, it is important to further understand the regulation and expression dynamics of collagen-binding integrins CD49a and CD49b *in vivo*. Based on known expression patterns as described above, we hypothesized that

CD49a and CD49b expression on CD8 T-cells is tightly regulated during antigen-driven differentiation, as well as by anatomical residence of the activated T-cell. To address this, we determined the dynamics of CD49a and CD49b integrin expression on CD8 T-cells during vaccine-induced and anti-tumor immune responses. Furthermore, we utilized adoptive transfer of specific integrin-expressing T-cell populations to track their differentiation over time in tumor-bearing hosts. We established separate roles of antigen-driven differentiation and elements in the TME in controlling the expression of CD49a and CD49b by CD8 T-cells. We also hypothesized that CD49a and CD49b play distinct roles in T-cell function by affecting T-cell location and motility. Therefore, we determined how expression of either integrin affects CD8 T-cell functional capacity in tumors and how expression correlated with the generation of exhausted and T_{RM} phenotypes. Our studies revealed a potentially important role for CD49a in T-cell motility and ability to engage with tumor cells.

METHODS

Mice

C57BL/6 mice were from Charles River/NCI. CD2-dsRed (kindly provided by Jordan Jacobelli at the University of Colorado, Anschutz Medical Campus), Nur77-GFP reporter (C57BL/6-Tg(Nr4a1-EGFP/cre)820Khog/J) (34), OT-I transgenic (C57BL/6-Tg(TcraTcrb)1100Mjb/J), and Thy1.1 congenic mice (B6.PL-Thy1a/CyJ) (Jackson Laboratories) were bred in-house in a pathogen-free facility. For tumor studies, male and female mice between 6-12 weeks of age were used. All procedures were approved by the University of Virginia Animal Care and Use Committee in accordance with the NIH Guide for Care and Use of Laboratory Animals.

Tumor lines and injections

BRPKp110 breast carcinoma cells (expressing GFP) were provided by Jose Conejo-Garcia and Melanie Rutkowski (35). B16-F1 cells were obtained from the American Type Culture Collection and transfected with cytoplasmic ovalbumin (OVA) as described(36). Cells ($4x10^5$) were injected subcutaneously (SC) in the neck scruff in 200ml Phosphate-Buffered Saline (PBS). All cell lines used for tumor injections were cultured a within 2-8 passages post thaw and testing for mycoplasma contamination.

In vitro T-cell activation and culture

Single cell suspension of spleens from OT-IxThy1.1 or C57BL/6 mice were filtered through 70m mesh (Miltenyi) and treated with red blood cell (RBC) lysis buffer (Sigma). CD8 T-cells were enriched with magnetic beads (Miltenyi) according to the manufacturer's protocol, and cultured at $1x10^6$ cells/ml in RPMI1640 with 10%

Fetal Bovine Serum (FBS) (Sigma), 15mM Hepes, 2mM L-glutamine, 10mM sodium pyruvate, 1X essential and non-essential amino-acids, 1mg/ml gentamicin (all from Gibco), 0.05mM β-mercaptoethanol (Sigma), 120 IU/ml human recombinant IL-2 and 10ng/ml murine recombinant IL-7 (Peprotech). CD3/CD28 T activator beads (Gibco) were added for the first 48h, after which they were magnetically removed. Cells were split to 1x10^6 cells/ml with fresh medium every 2-3 days.

Tumor lysates for addition to OT-I cell cultures were generated from day 28 BRPKp110 tumors. Tumors were harvested, cut into small pieces, resuspended in H$_2$O for 20 min, and sonicated on ice for 20 min (30 sec on, 30 sec off throughout) with a Sonic Dismembrator Model 500 (Fisher Scientific), amplitude of 37%. Lysates were centrifuged at 10,000 x g for 20 min at 4°C. Supernatants were collected, filtered through a 0.2m filter and supplemented with PBS containing 10% FBS (Sigma), 15mM Hepes, 2mM L-glutamine, 10mM sodium pyruvate, non-essential amino-acids, essential amino-acids, 1mg/ml gentamicin (all from Gibco) and 0.05mM β-mercaptoethanol (Sigma).

Vaccination and adoptive cell transfer

Single cell suspension of spleens from OT-IxThy1.1 mice were filtered through 70m mesh (Miltenyi), treated with RBC lysis buffer (Sigma), washed in PBS, and injected intravenously (IV) (5x10^4 cells) into naïve Thy1.2$^+$ C57BL/6 mice. The next day, mice were injected IV with 500mg ovalbumin (Sigma), 50mg anti-CD40 (BioXcell) and 100mg polyIC (InvivoGen). Five days post vaccination, filtered and RBC lysed single cell suspensions of spleens were depleted of CD49a$^+$ cells and subsequently enriched for CD49b$^+$ cells. Cells were incubated with biotinylated CD49a (Miltenyi) or CD49b (clone HMa2, Biolegend) specific antibodies for 15 min, washed in PBS supplemented with 0.5% BSA, 2mM EDTA, 2mM L-glutamine, 10mM sodium pyruvate, 1X essential and non-essential amino acids, and (concentration) dextrose, and incubated with anti-biotin microbeads (Miltenyi) for 15 min. Cells were then depleted (CD49a) or enriched (CD49b) with magnetic separation columns (Miltenyi). The fraction of Thy1.1$^+$ OT-I cells was quantitated and 1x10^6 Thy1.1$^+$ cells were injected IV into tumor bearing mice in 200ml PBS supplemented with 15,000U/ml IL2.

In vivo checkpoint inhibitor blockade

Mice were treated intraperitoneally with anti-PD-1 (clone RMP1, BioXCell), anti-LAG-3 (clone C9B7W, BioXCell), and anti-TIM-3 (clone RMT2-23, BioXCell) or matching IgG isotype controls (clones HRPN and 2A3, BioXCell) (250mg/mouse for each antibody) 48h prior to tumor harvest.

Tumor harvest

At indicated time points, tumors were harvested in RPMI-1640 supplemented with 2% FBS (Sigma), 15mM HEPES, 2mM L-glutamine, 10mM sodium pyruvate, 1X

essential and non-essential amino acids (all Gibco), 0.05mM b-mercaptoethanol (Sigma), 1mg/ml gentamicin (Gibco), 76mg/ml liberase TM (Roche) and 40mg/ml DNAse (Sigma). Tumors were digested for 15 min at 37°C and homogenized to a single cell suspension. The CD45 fraction was enriched with magnetic beads (Miltenyi) and the Miltenyi Automacs system.

Flow cytometry

Cells were Fc blocked (BioXcell), stained with Aqua Live/Dead dye and stained with fluorescently labeled antibodies (Supplemental Table 1). The BD Cytofix/ Cytoperm and BD Transcription Factor Staining kits were used for fixation/ permeabilization in intracellular and intranuclear stains, respectively. Cells were analyzed on Cytoflex (Beckman Coulter) or Attune (BD Biosciences) flow cytometers and analyzed with FlowJo software.

Live tumor slice imaging

Tumors were harvested and directly embedded in 2% low-melting point agarose. Tissue was cut into 100-200μm slices and placed in RPMI1640 without phenol red (Gibco). From each tumor, 3 slices were cut and either left untreated, treated with 10μg/ml purified CD49a antibodies (clone Ha/31, BD Biosciences) or 10μg/ ml purified CD49b antibodies (clone HMa2, BD Biosciences) for 2h at room temperature. Slices were mounted and stabilized in an imaging chamber under the microscope objective lens. Imaging was conducted using an in-line heating chamber with circulating media maintained in oxygenated RPMI1640 without phenol red (Gibco) at a flow rate of ~2ml/min. Cells were imaged using a two-photon microscope (Leica TCS SP8) with a Coherent Chameleon laser tuned to 880 nm with a 25X water-immersion lens (0.9NA). Fluorescence was detected using three photomultiplier tubes in whole-field detection mode and a 565nm dichroic mirror with 450/50nm (blue channel) 525/50nm (green channel) and 620/60nm (red channel) emission filters. The laser power was maintained at 25mW or below. We imaged cells between 78-84μm from the slice surface. Images were collected for at least 30 minutes. Typically, consecutive z-stack images were collected at 3μm intervals every minute. Movies were generated and processed using with Imaris software for analysis.

Statistical analysis

In flow cytometry experiments, when comparing integrin-expressing subpopulations, a Repeated-Measures one-way ANOVA with Tukey's multiple comparisons test was performed. When different time points, or treatment groups were tested, a Welch's corrected T-test was used. For imaging analyses of T-cell motility and distance to collagen or tumor cells, all T-cell spots for the slices evaluated were combined and compared amongst groups with an ordinary one-way ANOVA with Tukey's multiple comparisons test. Trends were confirmed by comparing groups with the same test for T-cell spots per tumor.

RESULTS

Identification of CD49a and CD49b expressing subpopulations of CD8 T cells in murine B16 melanoma and BRPKp110 breast tumor models

We previously showed that CD49a and CD49b integrins are expressed on CD8 tumor infiltrating lymphocytes (TIL) from human melanomas, but they are almost completely absent on CD8 T cells from normal donor PBMC or tumor-free lymph nodes from patients (31,37). Additionally, we showed that expression of these integrins identified human CD8 TIL subpopulations that varied in levels of perforin, CD127, PD-1, LAG-3 and TIM-3. To further elucidate the origin and evolution of these tumor-associated subpopulations, we utilized two implantable murine tumor models: collagen-rich breast cancer BRPKp110 and collagen-poor melanoma B16-F1 (38). In both models, we observed CD49aCD49b double negative (DN), CD49b single positive (SP), CD49aCD49b double positive (DP) and CD49a SP populations (Fig. 1B). Collagen-rich BRPKp110 contained proportionally more CD49a- and CD49b-expressing cells than collagen-poor B16-F1 (Fig. 1B). Although the CD49b SP subpopulation was more abundant in both murine models than in human TIL, the same subpopulations of retention integrin expressing cells were present in both mouse and human TIL, allowing us to further understand their characteristics.

CD49b- and CD49a-expressing CD8 T-cells appear sequentially after immunization and in the tumor microenvironment

To understand the regulation of CD49a and CD49b expression during an immune response, we evaluated ovalbumin-specific OT-I cells after ovalbumin (OVA) immunization. Early after activation (day 3), expression of CD49a and CD49b remained low and comparable to that of resting OT-I cells (Fig. 1C). By day 5, the fraction of OT-I cells expressing CD49b increased markedly, while the fraction expressing CD49a did not increase until day 9 (Fig. 1C, Supplemental Fig. 2A). By day 14, an overall decline in cells expressing CD49b was observed (Fig. 1C). Next, we quantitated CD49a and CD49b expressing subpopulations among CD8 TIL over the course of BRPKp110 tumor outgrowth. All 4 subpopulations were evident 14 and 23 days after tumor implantation (Fig. 1D). However, the fraction of CD49b SP cells was higher on day 14, while the fractions of CD49a SP cells and DP cells were increased at the later timepoint (Fig. 1E,F). These transitions in integrin-expressing subpopulations were accompanied by an early increase in the absolute number of CD49b SP and DP cells, followed by a decline in the CD49b SP cells and an increase in the absolute number of CD49a SP cells later in tumor development (day 23) (Fig. 1F). The absolute number of DN cells remained low and constant throughout. Collectively, these results establish that the four subpopulations identified in tumors are not stable, but arise sequentially during the course of an immune response.
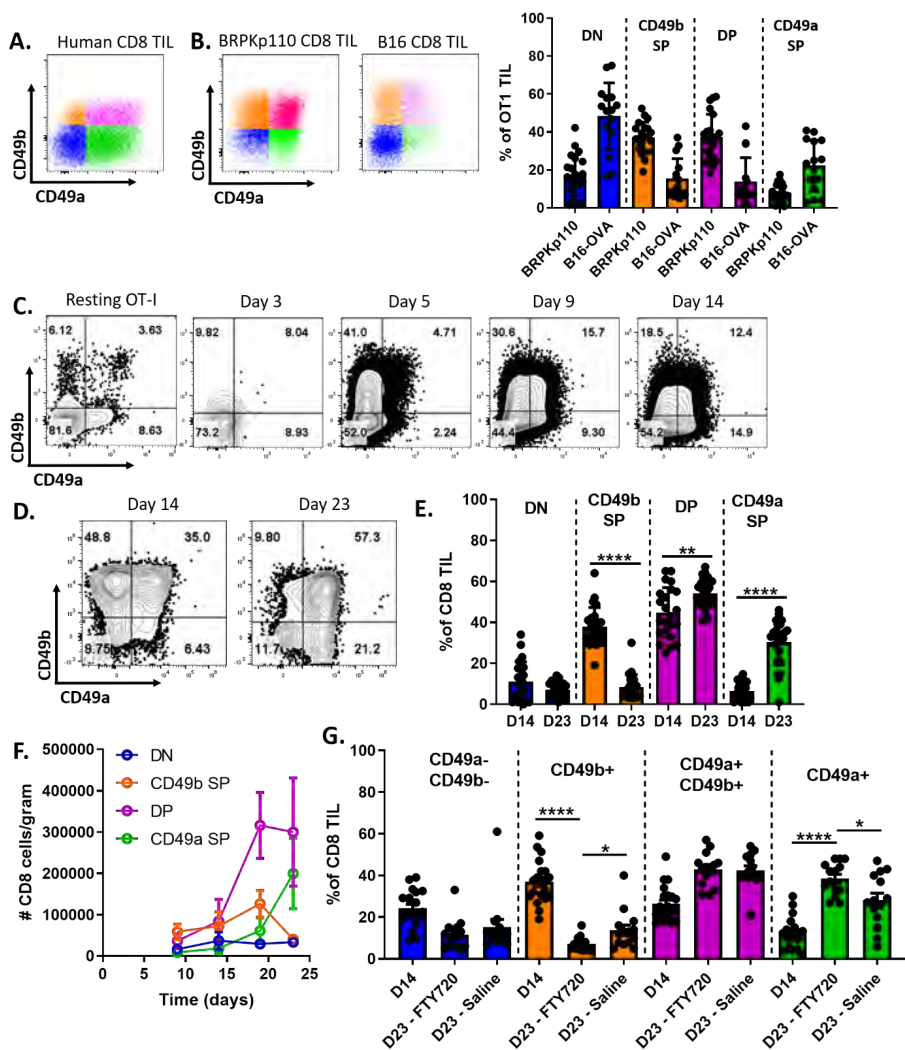
Figure 1: CD49b and CD49a expressing CD8 T-cells arise sequentially during immune responses induced by vaccination or tumor. (A) Single cell suspensions of human metastatic melanoma lesions were analyzed for CD49a and CD49b expression on CD3⁺CD8⁺ cells. (B) C57BL/6 mice were implanted SC with BRPKp110 breast carcinoma (n=21, 4 independent experiments) and murine B16-OVA melanoma (n=15, 3 independent experiments) samples. Tumors were harvested on day 14, single cell suspensions were prepared and enriched CD45⁺ cells were analyzed for CD49a and CD49b expression on CD3⁺ CD8⁺ cells. (C) Thy1.1⁺ OT-I splenocytes were transferred IV into C57BL/6 mice, which were subsequently immunized with OVA, polyIC, and anti-CD40. Baseline OT-I spleens (pre-transfer) or spleens harvested on the indicated days post transfer and vaccination (n=3 per time point) were analyzed for CD49a and CD49b expression on Thy1.1⁺ CD3⁺ CD8⁺ cells by flow cytometry. (D-G) Subcutaneous BRPKp110 tumors were harvested on the

indicated days, and the CD45$^+$ enriched fraction was analyzed for CD49a and CD49b expression on CD3$^+$ CD8$^+$ cells. (E) n=23-24, 5 independent experiments. Day 14 (D14) and day 23 (D23) were compared within each subset with a Welch's corrected T-test. (F) n=6-8 per time point from 2 independent experiments. (G) Groups of BRPKp110-bearing mice received daily IP injections with either saline or FTY720, starting on day 14 to block migration of additional T-cells from secondary lymphoid organs to the tumor. N=14-20 mice per group from 3 independent experiments. Groups were compared within subsets with a Welch's corrected T-test.

Change in integrin expression occurs specifically in the TME

Our results suggest either that CD49b and CD49a are sequentially expressed on CD8 TIL over the course of tumor outgrowth, or that separate subpopulations of CD8 T-cells with distinct integrin expression patterns are sequentially generated during vaccine-induced and anti-tumor immune responses. To test the latter hypothesis, we utilized FTY720 to block new T-cell infiltration from the periphery, starting on day 14 after tumor implantation. Despite that blockade, the proportion of CD49a SP cells still increased between day 14 and 23 (Fig. 1G). Interestingly, this increase was also significantly greater after FTY720 treatment compared to the saline control (Fig. 1G), potentially because the entry of new CD49b SP cells was also blocked. Together, these data suggest that CD49b SP cells differentiate into CD49a SP cells in the TME over time, with DP cells as a likely intermediate.

CD49a is upregulated on CD49b SP CD8 T-cells after they enter the TME

To interrogate if the TME drives upregulation of CD49a on CD49b SP cells independent of cognate antigen, we transferred CD49b SP cells into mice bearing OVA-negative tumors. First, mice that had been adoptively transferred with OT-I cells were immunized with OVA, leading to upregulation of CD49b on a substantial fraction of the OT-I cells (Fig. 1C). Five days post immunization, we purified CD49b SP OT-I cells from spleens and transferred them into either naïve, tumor-free or established (day 14), OVA-negative BRPKp110 tumor-bearing mice (Fig. 2A). Seven days post transfer, CD49b SP OT-I cells transferred into non-tumor bearing mice failed to upregulate CD49a and had significantly diminished expression of CD49b (Fig. 2B). This contrasts with the behavior of these cells in the original immunized mice, in which CD49a was upregulated over time (Fig. 1C). CD49b SP OT-I cells transferred into mice with BRPKp110 tumors trafficked to tumors consistently and numerously, despite the lack of OVA expression (Fig. 2C). CD49a was expressed on 50-60% of the intratumoral OT-I cells within 24h and virtually all cells expressed CD49a after 7 days (Fig. 2D). At early time points most of the cells were DP, but a CD49a SP subpopulation was evident after 7 days, suggesting DP OT-I cells lose CD49b over time (Fig. 2D). Importantly, transferred CD49b SP OT-I cells isolated from the spleens of these tumor-bearing mice never upregulated CD49a, and showed a significantly lower CD49b expression (Fig. 2E,F), similar to the behavior seen in non-tumor bearing mice (Fig. 2B).
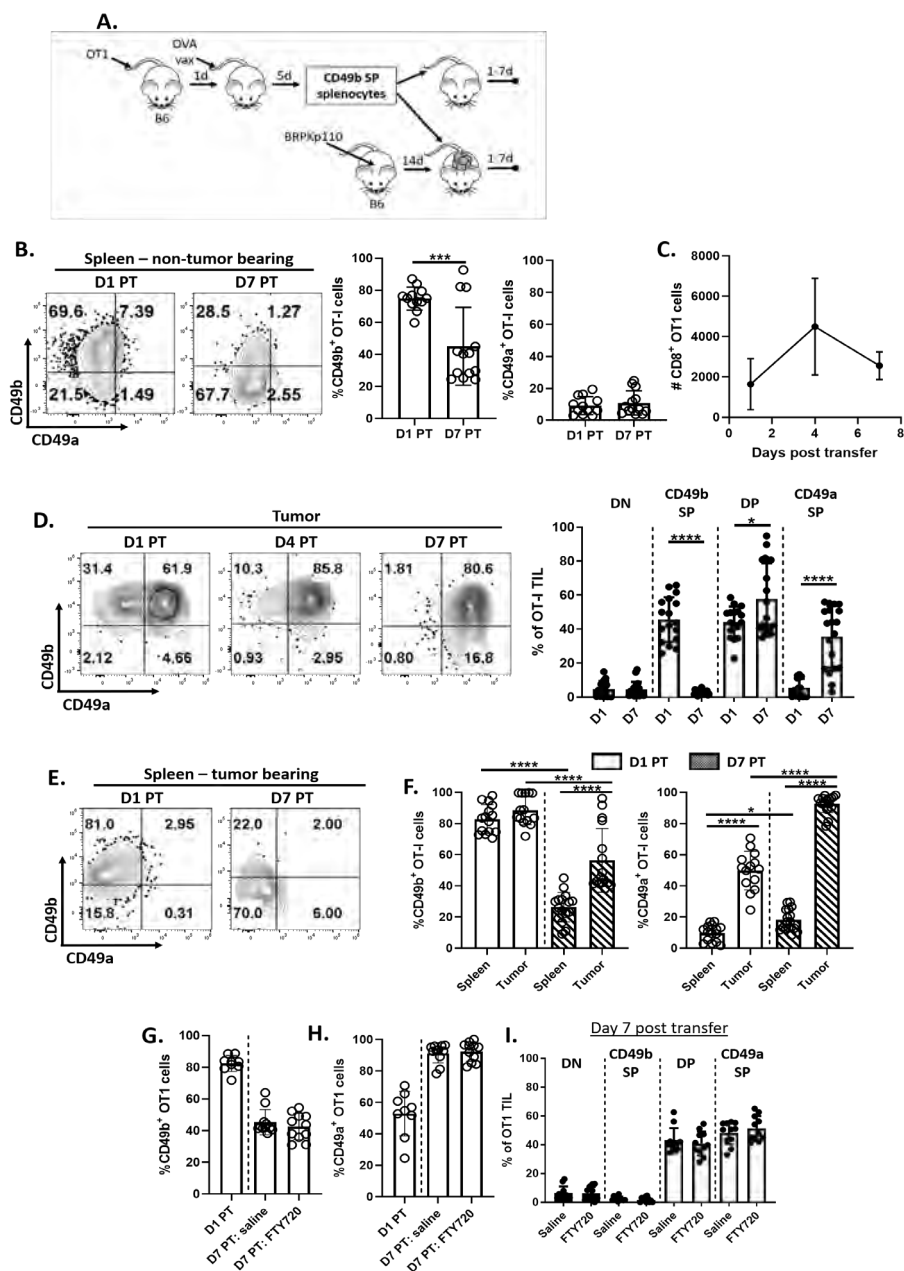
Figure 2: CD8 T-cell differentiate in a stepwise manner from a CD49b SP to DP to CD49a SP in the TME. (A) Schematic of experimental immunization and adoptive transfer model. Details are in Methods and Results. (B) Spleens from tumor-free mice were harvested 1 or 7 days post transfer (PT) of CD49b SP Thy1.1+ OT-I effectors and analyzed for CD49a and CD49b expression on Thy1.1+ CD3+ CD8+ cells by flow cytometry (n=12-13 from 4 independent

experiments, groups were compared with a Welch's corrected T-test). (C-I) Tumors or spleens from BRPKp110 tumor-bearing mice were harvested on the indicated days post transfer (PT) of CD49b SP Thy1.1^{+} OT-I effectors. Tumor suspensions were enriched for CD45^{+} cells and the number of accumulated Thy1.1^{+} CD3^{+} CD8^{+} cells (C, n=6 per time point, 2 independent experiments) and CD49b and CD49a expression on accumulated Thy1.1^{+} CD3^{+} CD8^{+} cells (D, F, G, H, I; n=17-19 per time point from 4 independent experiments) was evaluated by flow cytometry. Time points in (D) were compared in each subpopulation with a Welch's corrected T-test. Splenocytes were analyzed for CD49a and CD49b expression on Thy1.1^{+} CD3^{+} CD8^{+} cells by flow cytometry (E, F). Comparisons in (E) were done with an ordinary one-way ANOVA. (G-I) Thy1.1^{+} OT-I splenocytes were activated and transferred IV into BRPKp110-bearing C57BL/6 mice, as described in (A). Mice received daily IP injections FTY720 or saline control starting at day 1 PT, to block migration of additional T-cells from secondary lymphoid organs to the tumor. Tumors were harvested on day 7 post transfer and enriched CD45^{+} fractions were analyzed for CD49b and CD49a expression on Thy1.1^{+} CD3^{+} CD8^{+} cells (n=9-11 per group from 2 independent experiments).

These data did not exclude the possibility that OT-I cells upregulated CD49a elsewhere in the animal, and then infiltrated the tumor. To test this latter possibility, we transferred CD49b SP activated OT-I cells into BRPKp110 tumor-bearing mice and treated them with FTY720 starting 1 day post transfer. Despite reducing CD8 T-cell numbers in the blood (Supplemental Fig. 3A), FTY720 had no impact on the number of tumor-infiltrating OT-I cells (Supplemental Fig. 3B). Additionally, FTY720 treatment did not change the reduction in CD49b expression (Fig. 2G) and the induction of CD49a expression on OT-I TIL (Fig. 2H), or the overall proportions of SP and DP OT-I cells in the spleen or tumor (Fig. 2I, Supplemental Fig. 3C). This demonstrates that CD49a is upregulated on CD49b SP cells after they enter the tumor. Overall, our data indicate that activation-induced differentiation of CD8 T-cells is insufficient to induce CD49a, and that this is instead dependent on an environmental factor, present both in spleens of immunized mice and the TME, that upregulates CD49a independent of antigen-stimulation.

A soluble factor in the TME upregulates CD49a expression on CD8 T-cells

We hypothesized that the mediator(s) responsible for CD49a upregulation might be intrinsic to the tumors. To test this, we cultured *in vitro* activated OT-I cells with lysates from 28-day old BRPKp110 tumors. The lysate upregulated CD49a on most of these cells within 24h, independent of CD49b status, and without apparent change in CD49b expression (Fig. 3A). Since CD49a is upregulated on activated human CD8 T-cells *in vitro* by TGFβ(31), *in vitro* activated OT-I cells were cultured with BRPKp110 tumor lysates in the presence of TGFβ1-3 blocking antibodies. However, there was no difference in CD49a upregulation (Fig. 3B). Blocking TGFβ1-3 with the same antibodies during BRPKp110 tumor outgrowth *in vivo* only modestly diminished the fraction of CD49a^{+} CD8 TIL (Supplemental Fig. 4A). Additionally, culturing *in vitro* activated OT-I cells with recombinant TGFβ1 did not induce CD49a expression, although it did diminish CD49b expression (Fig.

3B, Supplemental Fig. 4B). Thus, a soluble factor other than TGFβ that is present in tumor lysates upregulates CD49a expression on CD8 T-cells *in vitro* and is likely responsible for induction of CD49a on CD8 TIL *in vivo*.
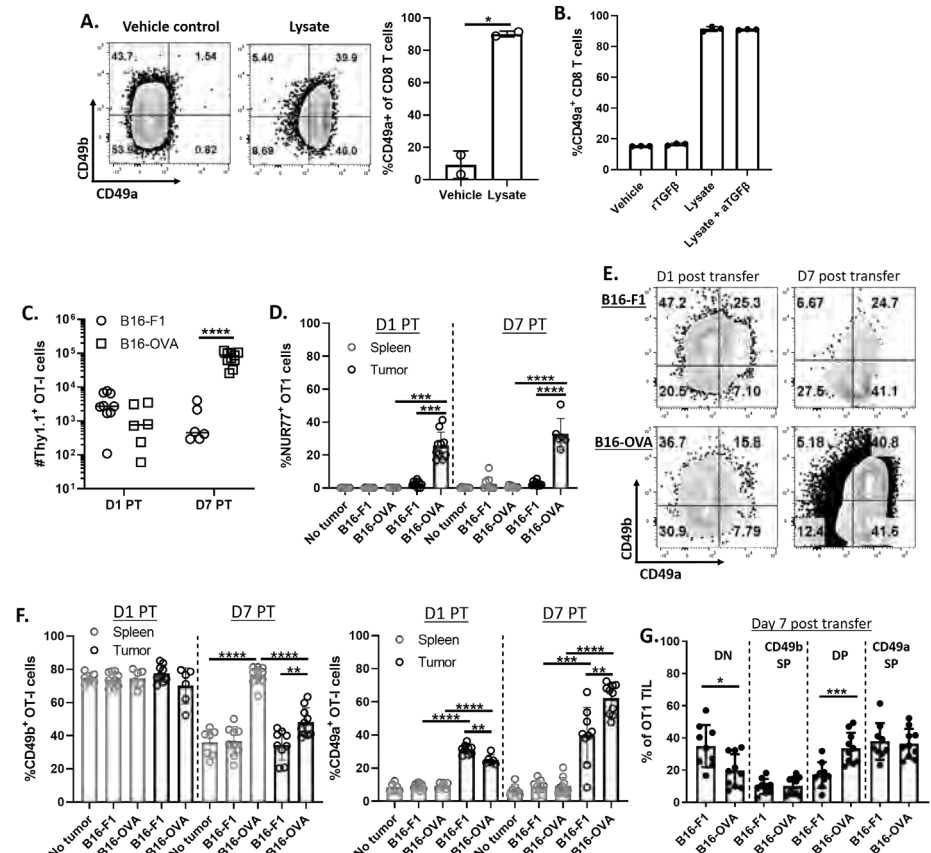

Figure 3: Soluble tumor-derived factors are responsible for upregulation of CD49a. (A, B) Thy1.1+ CD8+ OT-I cells were activated with CD3/CD28 activation beads, cultured in presence of IL-2 and IL-7, and then cultured for 24h with BRPKp110-derived tumor lysate (A) or recombinant human TGFβ1, BRPKp110 tumor lysate, or tumor lysate with added TGFβ blocking antibody (B). Cells were evaluated for CD49a expression by flow cytometry. (C-G) Thy1.1+ OT-I Nur77-GFP reporter splenocytes were transferred into C57BL/6 mice that were subsequently immunized with OVA, polyIC, and anti-CD40, and CD49b SP Thy1.1+ OT-I effectors isolated and transferred into B16-F1 or B16-OVA tumor-bearing or tumor-free mice as in Figure 2A. Tumors or spleens from tumor-bearing mice were harvested 1 or 7 days post transfer and the number of accumulated Thy1.1+ CD3+ CD8+ cells (C), and Nur77-GFP expression (D) and CD49b and CD49a expression (E-G) on accumulated Thy1.1+ CD3+ CD8+ cells evaluated by flow cytometry. Each time point and group contained n=6-10 from 2 independent experiments and direct comparisons between groups within a time point were tested with a Welch's corrected T-tests.

Antigen stimulation augments environmentally-induced expression of CD49a

We next addressed the impact of TCR stimulation on the expression of CD49a and CD49b integrins, beyond the early TCR-induced upregulation of CD49b. BRPKp110 expresses very low levels of MHC-I molecules, and BRPKp110 transfected with OVA is very poorly recognized by OT-I cells *in vitro* and *in vivo* (not shown). Consequently, activated CD49b SP OT-I cells were transferred into mice bearing B16-F1 melanomas, either non-transfected or transfected to express OVA (B16-F1 and B16-OVA, respectively). These OT-I cells came from Nur77-GFP reporter mice, enabling us to measure TCR signaling in the transferred population. OT-I cells trafficked into both types of tumors, but their number was substantially increased over 7 days when tumors expressed OVA (Fig. 3C). A significant fraction of cells transferred into B16-OVA tumor-bearing mice upregulated Nur77, indicating local activation by antigen, whereas no Nur77 was expressed in OT-I cells isolated from spleens of B16-OVA bearing-mice or in spleens and tumors of B16-F1 bearing-mice (Fig. 3D). In B16-F1 tumor-bearing mice, OT-I cells lost CD49b in spleen and tumor comparably (Fig. 3E,F). Thus, in contrast to the BRPKp110 TME (Fig. 2D), the B16-F1 TME does not support CD49b maintenance. In B16-OVA tumor-bearing mice, CD49b was maintained on OT-I cells in the spleen, and lost in the TME, although not to the same extend as in B16-F1 tumors (Fig. 3E,F). These results suggest that TCR stimulation not only upregulates CD49b, but also maintains its expression. However, aspects of the TME, such as TGFβ1 or continuous antigen exposure, may diminish CD49b expression. As was observed in BRPKp110 tumors, CD49a was upregulated on CD49b SP OT-I cells in B16 tumors but not spleens of tumor-bearing mice, and this occurred regardless of antigen (Fig. 3F,G). However, the upregulation was significantly greater by day 7 in B16-OVA than B16-F1 tumors. Although it is possible that B16-OVA could support the selective proliferation of CD49a-expressing subpopulations, a more likely explanation is that antigen stimulation augments the TME-dependent upregulation of CD49a expression.

Expression of exhaustion markers is not linked to differential expression of CD49b and CD49a

CD8 TIL become exhausted over time due to chronic antigen stimulation(39). Since both the TME and antigen stimulation drove CD49a upregulation, we determined how CD49a expression and expression of exhaustion markers PD-1, LAG-3 and TIM-3 were associated. Due to the low numbers of transferred cells recovered from BRPKp110 and B16-F1 tumors, it was not possible to evaluate this association as driven by the TME in the absence of antigen. However, we did evaluate integrin-expressing subpopulations arising after transfer of CD49b SP OT-I cells into B16-OVA tumor bearing mice. At the time of transfer, CD49b SP OT-I cells adoptively transferred into tumor-free or B16-OVA tumor-bearing mice expressed PD-1 uniformly, but expressed low levels of LAG-3 and TIM-3, consistent with an effector T-cell phenotype (Fig. 4A). Seven days after transfer into tumor-free mice, a fraction of OT-I cells in the spleen had lost PD-1 expression

and the gMFI on the remaining PD-1$^+$ OT-I cells was substantially lower (Fig. 4B). Expression of LAG-3 and TIM-3 on OT-I, though already low at time of transfer, was decreased further. In B16-OVA tumor-bearing mice, exhaustion marker expression on splenic OT-I cells 7 days after transfer was similar to that of tumor-free mice (Fig. 4C). In contrast, PD-1 expression was maintained on all OT-I cells that infiltrated B16-OVA tumors while the MFI was also substantially increased. They also upregulated LAG-3 and TIM-3. These results establish that adoptively transferred CD49b SP OT-I cells acquire an exhausted phenotype based on residency in an antigen-expressing TME. To test whether the upregulation of CD49a was associated with generation of an exhausted phenotype, we evaluate PD-1, LAG-3 and TIM-3 expression on each integrin-expressing OT-I subpopulation, 7 days post transfer. Compared to CD49b SP OT-I phenotype at the time of transfer, PD-1 remained expressed on essentially all cells in all 4 subpopulations, and TME-induced upregulation of the level of expression was also consistent (Fig. 5A). The percentage of DP cells expressing LAG-3 and TIM-3 was very slightly but significantly higher than that of CD49b SP and DN cells, but there was no further increase in the CD49a SP population (Fig. 5A). Similarly, when naïve OT-I cells were transferred prior to B16-OVA implantation and thus activated *in vivo* by tumor-derived OVA, these exhaustion markers were not differentially expressed among integrin-expressing subpopulations (Supplemental Fig. 5). These results suggest that acquisition of an exhausted phenotype is largely independent of CD49a expression.

We also examined the endogenous CD8 T-cells from the same B16-OVA tumors analyzed above, as well as endogenous CD8 T-cells from BRPKp110 and B16-F1 tumors. In contrast to the results above, the fractions of endogenous DP and CD49a SP subpopulations expressing PD-1, LAG-3, Tigit and/or TIM-3 in B16-OVA and BRPKp110 tumors were significantly higher than that of the CD49b SP cells, as was the gMFI of PD-1 (Fig. 5B,C). These same trends were observed in B16-F1 tumors, although the fractions of the subpopulations expressing PD-1 were not different (Fig. 5D). However, the CD49a SP subpopulation only significantly differed from the DP population in B16-OVA tumors, and only in relation to expression of PD-1 and LAG-3. Thus, there is an association between the gain of an exhausted-like phenotype and CD49a expression on endogenous CD8 TIL. As described earlier (Fig. 1G), endogenous T-cells are likely infiltrating into tumors continuously, in contrast to transferred OT-I cells. Endogenous CD49b SP cells are therefore "newer" on average and for that reason, less exhausted. This suggests that the association between integrin differentiation and an exhausted phenotype on endogenous CD8 TIL is temporal, but not mechanistically linked.

A. Activated CD49b SP OT-I, pre-transfer from spleen
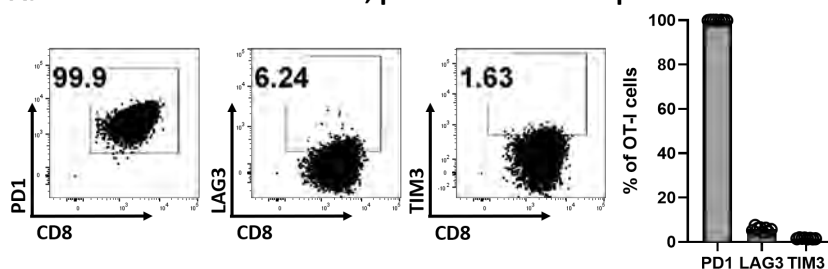
B. Activated CD49b SP OT-I, spleen 7 days post transfer
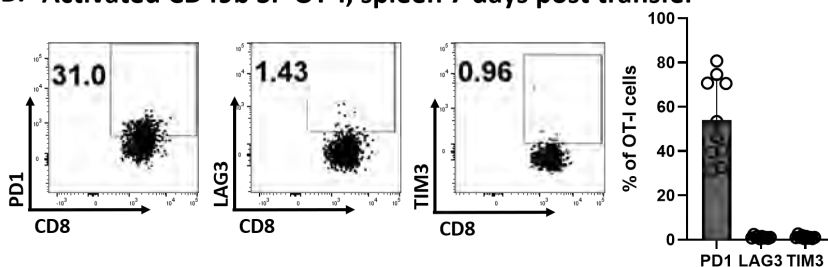
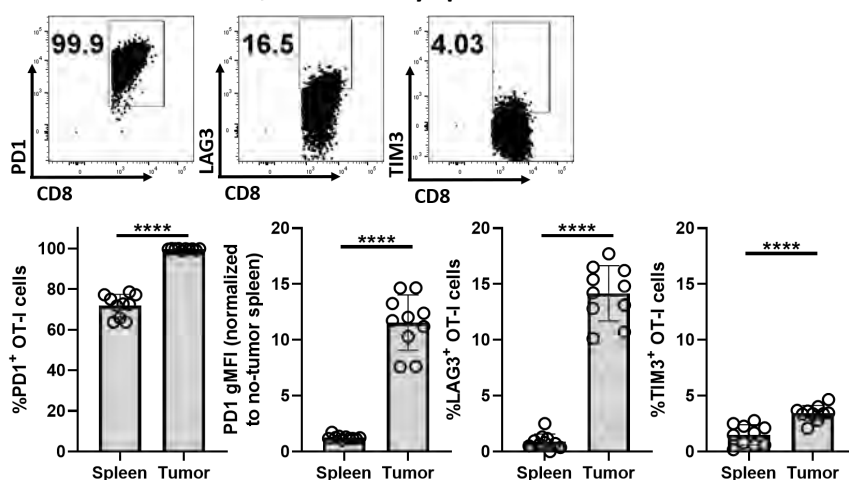## C. OT-I in B16-OVA, tumor 7 days post transfer

Figure 4. Exhaustion marker expression is driven by environment and antigen-driven differentiation. Experiments were set up as in Figure 2A. Expression of PD-1, LAG-3, TIM-3 and Tigit on isolated CD49b SP Thy1.1[+] OT-I cells were determined by flow cytometry. (A) 5 days after vaccination, and prior to transfer. (B) Seven days after transfer into tumor-free mice. (C) Seven days after transfer into B16-OVA tumor-bearing mice (n=10 from 2 independent experiments). Exhaustion marker expression between spleens and tumors were compared with a Paired T-test.
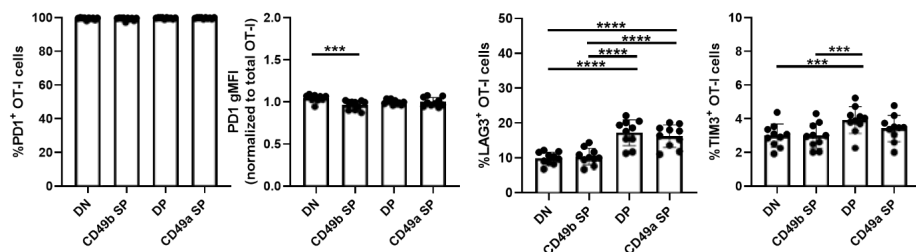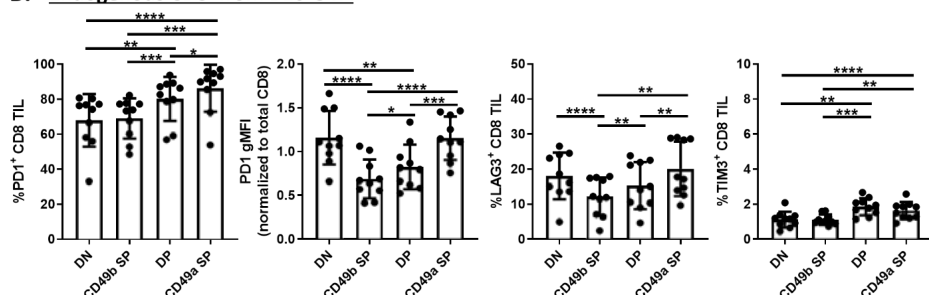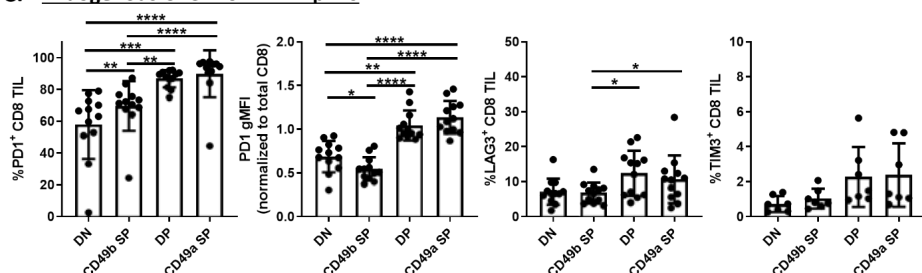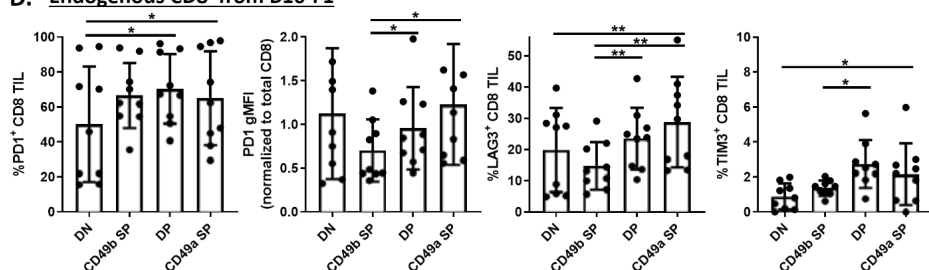
Figure 5: Progression of integrin expression is linked to gain of exhaustion phenotype on endogenous CD8 T-cells. Experimental details were as in Figure 2A. The indicated exhaustion markers were evaluated on either Thy1.1^{+} OT-I cells isolated from B16-OVA tumors seven days after transfer (A), or endogenous Thy1.1^{neg} CD3^{+} CD8^{+} cells isolated from the same B16-OVA (B; n=10), B16-F1 (C; n=9) and BRPKp110 (D; n=12) tumors evaluated in Fig. 4C-E. Marker expression between subpopulations was compared with a Repeated Measures one-way ANOVA and Tukey's multiple comparisons test.

CD49b SP cells can engage with antigen, whereas TCR signaling is low or absent in DP and CD49a SP cells

Based on the elevated expression of exhaustion markers on endogenous CD49a$^+$ CD8 T-cells, we hypothesized that these cells would be less functional *in vivo*. To test this, BRPKp110 tumors were implanted into Nur77-GFP reporter mice. As hypothesized, DP and CD49a SP subpopulations showed significantly less TCR signaling than CD49b SP cells, as measured by Nur77 expression (Fig. 6A, Supplemental Fig. 6A). In fact, Nur77 expression in the CD49a SP cells was not higher than the baseline expression in CD8 T-cells from non-draining lymph nodes. Irrespective of CD49a or CD49b expression, no CD8 TIL expressed IFNg or TNFa directly *ex vivo* after *in vivo* brefeldin A treatment 4-6h prior to harvest (Fig. 6B). However, significant fractions expressed IFNγ, TNFα and surface CD107a after *in vitro* restimulation for 4-6h with anti-CD3/CD28, demonstrating that they are active outside the context of a tumor (Fig. 6C, Supplemental Fig. 6B). Interestingly, IFNg, CD107a and TNFa were expressed on larger fractions of DP cells than either SP subpopulation. Importantly, all subpopulations upregulated Nur77 equivalently upon re-stimulation for 12 hours with anti-CD3/CD28 *in vitro* (Fig. 6D). These data demonstrate that, while all subpopulations are suppressed downstream of Nur77 *in vivo*, CD49b SP cells are able to engage with antigen and express Nur77, whereas CD49a SP cells are not. This suggest that either these subpopulations are suppressed by different mechanisms or that CD49a SP T-cells are not actively engaged with antigen.

As CD49a SP and DP T-cells expressed higher levels of exhaustion markers, we hypothesized that these inhibitory pathways suppressed TCR signaling more in these subpopulations. To test this, we treated established BRPKp110 tumors with a cocktail of checkpoint blockade inhibitors for 48h. Due to the short nature of treatment, tumor weight, CD8 T-cell infiltration, and CD49a and CD49b expression were unaltered (Supplemental Fig. 6C). However, neither Nur77 expression (Fig. 6E) nor effector cytokine expression was changed (Fig. 6F), indicating that blockade of inhibitory signaling via PD-1, LAG-3, or TIM-3 could not rescue effector activity or Nur77 expression of CD49a SP and DP T-cells in BRPKp110 tumors.
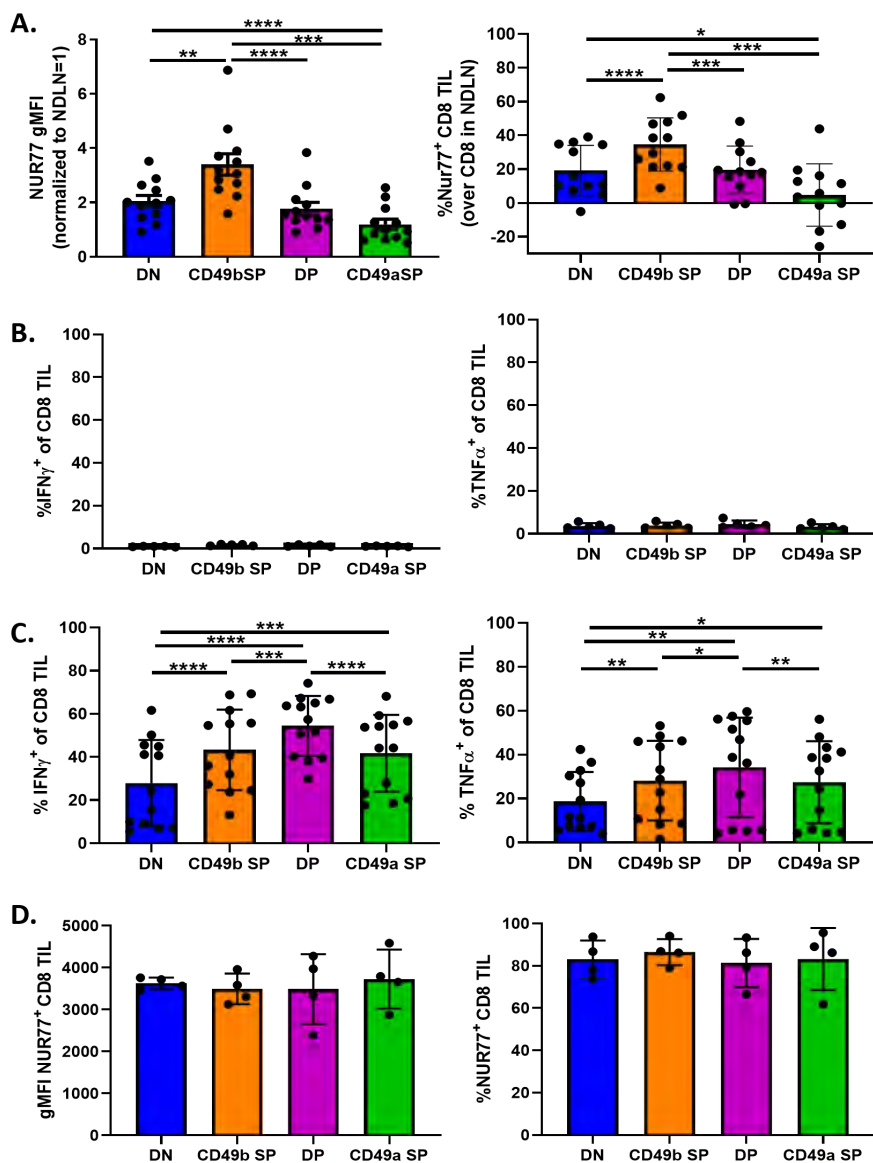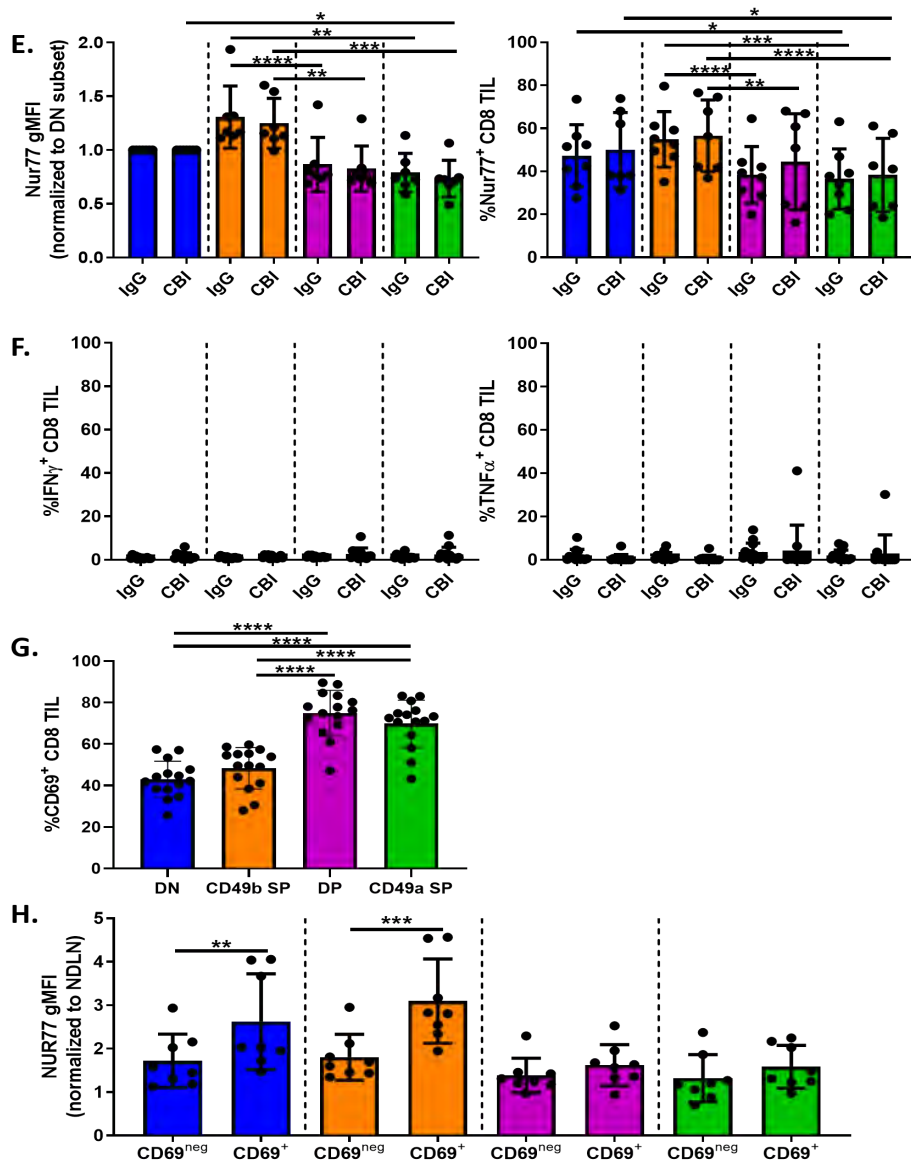
Figure 6. CD49a-expressing subpopulation are not inhibited by PD-1, LAG-3 or TIM-3, instead they display a TRM-like phenotype. (A) Nur77-GFP reporter mice were implanted SC with BRPKp110 (n=12 from 3 independent experiments). Tumors were harvested on day 14, single cell suspensions were prepared and enriched CD45 fraction was analyzed for Nur77-GFP, CD49a and CD49b expression on CD3$^+$ CD8$^+$ cells. Nur77 gMFI was normalized to CD8 T-cells in non-draining lymph nodes (NDLN) and Nur77% on CD8 T-cells from NDLN (ranging between 17.1-41.8%) was subtracted from the fraction on CD8 TIL subpopulations. Subpopulations were compared with a Repeated-Measures

E.

Nur77 gMFI (normalized to DN subset)

2.0, 1.5, 1.0, 0.5, 0.0

IgG CBI IgG CBI IgG CBI IgG CBI

* ** **** ** ***

%Nur77$^+$ CD8 TIL

100, 80, 60, 40, 20, 0

IgG CBI IgG CBI IgG CBI IgG CBI

* * *** **** ** ****

F.

%IFNγ$^+$ CD8 TIL

100, 80, 60, 40, 20, 0

IgG CBI IgG CBI IgG CBI IgG CBI

%TNFα$^+$ CD8 TIL

100, 80, 60, 40, 20, 0

IgG CBI IgG CBI IgG CBI IgG CBI

G.

%CD69$^+$ CD8 TIL

100, 80, 60, 40, 20, 0

DN   CD49b SP   DP   CD49a SP

**** **** **** ****

H.

NUR77 gMFI (normalized to NDLN)

5, 4, 3, 2, 1, 0

CD69^{neg} CD69$^+$ CD69^{neg} CD69$^+$ CD69^{neg} CD69$^+$ CD69^{neg} CD69$^+$

** ***

ANOVA. (B) C57BL/6 mice were implanted SC with BRPKp110 tumors (n=5). Tumors were harvested on day 14, 4-6h after IV injection of Brefeldin A. Single cell suspensions were prepared and enriched CD45 fraction was analyzed for CD49a, CD49b, IFNγ and TNFα expression on CD3$^+$ CD8$^+$. (C) C57BL/6 mice were implanted SC with BRPKp110 (n=13 from 2 independent experiments). Tumors were harvested on day 14, single cell suspensions were prepared and enriched CD8$^+$ cells were cultured with CD3/CD28 beads for 4-6h in presence of Brefeldin A. Cells were analyzed for expression CD49a, CD49b, IFNγ and TNFα expression on CD3$^+$ CD8$^+$. Expression between subpopulations was compared with a Repeated-Measures one-way ANOVA and Tukey's multiple comparisons test. (D)

Nur77-GFP reporter mice were implanted SC with BRPKp110 breast carcinoma (n=4). Tumors were harvested on day 14, single cell suspensions were prepared and enriched CD8$^+$ cells were cultured with CD3/CD28 beads for 12h and analyzed for Nur77-GFP, CD49a and CD49b expression CD3$^+$ CD8$^+$ cells. Expression between subpopulations was compared with a Repeated-Measures one-way ANOVA and Tukey's multiple comparisons test. (E/F) Nur77-GFP reporter mice were implanted SC with BRPKp110 (n=7 per group, 2 independent experiments). Mice were IP injected 48h prior to harvest with a checkpoint blockade inhibitor (CBI) cocktail including anti-PD-1, anti-LAG-3 and anti-TIM-3. Tumors were harvested, single-cell suspensions were prepared and enriched CD45 fraction was analyzed for Nur77-GFP, CD49a, CD49b, IFNγ and TNFα expression on CD3$^+$ CD8$^+$ cells. (G) C57BL/6 mice were implanted SC with BRPKp110 (n=15 from 3 independent experiments). Tumors were harvested on day 14, single cell suspensions were prepared and enriched CD45$^+$ cells were analyzed for CD69, CD49a and CD49b expression on CD3$^+$ CD8$^+$ cells. Expression between subpopulations were statistically compared as in (A) and differences between groups within a subpopulation were tested with a Welch's corrected T-test. (H) Nur77-GFP reporter mice were implanted SC with BRPKp110 breast carcinoma (n=8 per group, 2 independent experiments). Tumors were harvested on day 14, single cell suspensions were prepared and enriched CD45$^+$ cells were analyzed for Nur77, CD69, CD49a and CD49b expression on CD3$^+$ CD8$^+$ cells. CD69$^+$ and CD69^{neg} subsets within the integrin-expressing subpopulations were compared with a Paired T-test.

CD49a-expressing subpopulations express elevated levels of CD69 in an antigen-independent manner

While extrinsic suppression mechanisms, such as myeloid-derived suppressor cells or regulatory T-cells, could be responsible for the selective inhibition of TCR signaling in CD49a-expressing subpopulations, this would require that these cell types be differentially localized in proximity to one another. This led us to consider a more straightforward possibility: that CD49a-expressing subpopulations were localized away from antigen-expressing cells in the tumor and thereby able to functionally resemble a T$_{RM}$-like T-cell population. CD49a has been described as a marker of T$_{RM}$ cells, along with PD-1 and CD69 (40,41). Consequently, we evaluated CD69 expression on integrin-expressing subpopulations in conjunction with their expression of Nur77. All integrin-expressing subpopulations expressed CD69, though the fraction of CD69$^+$ cells was elevated in DP and CD49a SP subpopulations (Fig. 6G). In CD49b SP and DN subpopulations, these CD69$^+$ cells expressed elevated levels of Nur77, tying CD69 expression to TCR stimulation (Fig. 6H). However, in DP and CD49a SP subpopulations, there was no difference in Nur77 expression between CD69 positive and negative cells. This TCR-stimulation independent expression of CD69 is consistent with the antigen-independent expression of CD69 in T$_{RM}$ cells, and further consistent with the possibility that CD49a SP and DP cells are not in contact with antigen-expressing cells in the tumor

CD49a, but not CD49b, ligation alters T-cell localization and interaction with tumor cells resulting in high motility

The results above led us to consider that the engagement of CD49a with collagen reduced the ability of CD8 T-cells to engage with antigens expressed on tumor cells. To test this hypothesis, we implanted GFP-expressing BRPKp110 cells into CD2-dsRed (labeling all T-cells) transgenic mice. The resulting tumors were cut into 100-200µm thick live tumor slices, and tumor cells, CD2$^+$ T-cells, and collagen fibers identified by second harmonic generation (SHG) were imaged with 2-photon microscopy for 30 minutes at 37°C. Separate slices from the same tumors were incubated with blocking antibodies against CD49a or CD49b prior to imaging. Under control conditions, T-cells displayed a wide range of speeds and relatively few were slow-moving (<1µm/min) (Fig. 7A,B, Supplemental Fig. 7A, Supplemental Video 1-3). Only 5% of T-cells were <10 mm from a collagen fiber (Fig. 7C). However, SHG enables visualization only of well-structured collagen fibers (42,43). Immunofluorescent staining of day 21 BRPKp110 sections for collagen type I or IV confirmed a more pervasive presence of collagen molecules compared to that observed by SHG (Supplemental Fig. 7B), suggesting our live-imaging underestimates the true fraction of collagen-engaged cells. Nonetheless, those few cells in close proximity to visible collagen fibers moved significantly slower (Fig. 7D). In untreated tumors, about 22% of T-cells were <10mm from a tumor cell (Fig. 7E). However, no difference in speed was observed when comparing these T-cells to those located further away from collagen fibers (Fig. 7F, Supplemental Fig. 7E). These characteristics are consistent with a low level of productive tumor cell engagement (44,45). When CD49b was blocked, significantly more cells were located in closer proximity to tumor cells (Fig. 7E), but their track speed remained the same as T-cells at a distance, suggesting no change in their interaction (Fig. 7F, Supplemental Fig. 7C). Also, neither proximity nor track speed, overall or in relation to well-structured collagen fibers, was altered (Fig. 7A-D, Supplemental Fig. 7A, Supplemental Video 1-3). In contrast, CD49a blockade resulted in a significant decline in average T-cell motility (Fig. 7A,B, Supplemental Fig. 7A, Supplemental Video 1-3). Curiously, a significantly larger fraction of T-cells was in close proximity to well-structured collagen fibers but not to tumor cells (Fig. 7A-C). However, in contrast to control slices, the CD49a blocked T-cells in close proximity to tumor cells were moving significantly slower than those at a distance (Fig. 7F, Supplemental Fig. 7C), suggesting that their engagement was enhanced. This decrease in speed was not due to a larger fraction of T-cells interacting with both collagen and tumor cells simultaneously (Supplemental Fig. 7D): only T-cells close to tumor cells, and not those close to collagen fibers, showed significantly decreased speed when CD49a was blocked (Supplemental Fig. 7E). These data suggest that CD49a on T-cells either increases motility, which diminishes productive engagement with tumor cells. Alternatively, CD49a may diminish the ability of T-cells to productively engage with tumor cells, resulting in an increased T cell motility. Regardless, they point to a mechanism in which CD49a inhibits T-cell function by blocking the engagement with tumor cells.
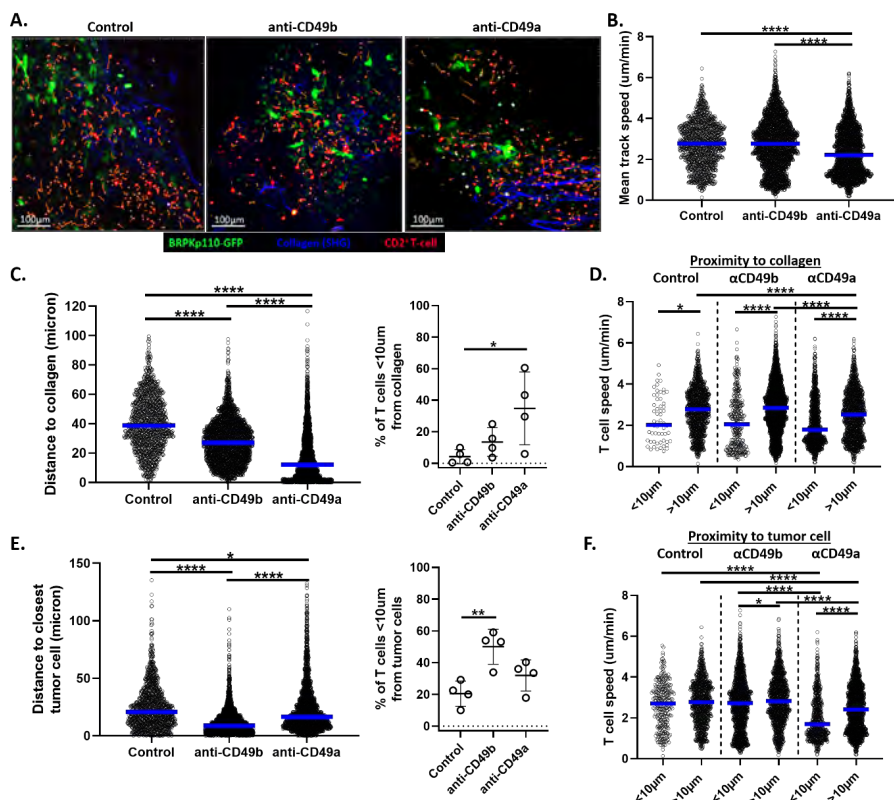
Figure 7. CD49a affects localization and motility of T-cells in the tumor. CD2-dsRed mice were implanted SC with BRPKp110-GFP tumors. Tumors were harvested on day 21/22, embedded in agarose and cut into thick slices of approximately 100-200µicrons. Slices were incubated with anti-CD49a or anti-CD49b blocking antibodies for 2h and assessed for CD2⁺ T-cells, GFP⁺ BRPKp110 cells and collagen fibers with second harmonics generation (SHG) on a 2-photon microscope. 30-minute videos of 2 fields per slice were made while maintaining oxygenation and 37°C with warm flowing media. For each figure, groups were compared with an ordinary one-way ANOVA and Tukey's multiple comparisons test. (A) Composite image examples. Orange tracks represent CD2⁺ T-cell movement for the last 10 minutes. (B) Mean track speed of the CD2⁺ T-cells. (C) Average distance of CD2⁺ T-cells to closest SHG collagen fiber (left). Fraction of CD2⁺ T-cells <10µm to closest SHG collagen fiber (right), fraction displayed per analyzed field. (D) Mean track speed of the CD2⁺ T-cells, stratified by distance to SHG collagen fibers. Close proximity: <10µm, large distance: >10µm. (E) Average distance of CD2⁺ T-cells to closest GFP⁺ BRPKp110 tumor cell (left). Fraction of CD2⁺ T-cells <10µm to closest GFP⁺ BRPKp110 tumor cell (right), fraction displayed per analyzed field. (F) Mean track speed of the CD2⁺ T-cells, stratified by distance to GFP⁺ BRPKp110 tumor cells. Close proximity: <10µm, large distance: >10µm.

DISCUSSION

Successful anti-tumor immune responses depend on robust T-cell infiltration in the tumor. Retention mechanisms may be involved in defining the extent of the T-cell infiltrate. The collagen-binding integrins CD49a and CD49b are considered to be involved in the retention of T-cells in peripheral tissues, including tumors (31). Thus, their regulation and function on T-cells in the TME may impact tumor control. Here, we found that CD8 T-cells express CD49b early after infiltration into tumors and then, over the course of tumor outgrowth, gain CD49a, and subsequently lose CD49b. This differentiation sequence is driven by antigen-independent elements in the TME, but antigen stimulation further enhances CD49a expression. CD49a-expressing CD8 TIL also expressed higher levels of PD-1, LAG-3, TIM-3 and Tigit, but these exhaustion markers were also upregulated on CD49a^{neg} CD8 TIL. Our work suggests that exhaustion markers and CD49a are associated temporally, but not mechanistically. On the other hand, CD49a-expressing CD8 TIL expressed CD69 in the absence of TCR signaling while its expression on CD49b populations was TCR signaling-associated. Co-expression of CD69 and CD49a is characteristic of T$_{RM}$ cells; thus, upregulation of CD49a may be associated with establishment of T$_{RM}$-like TIL that are not actively engaging with antigen. Unexpectedly, imaging T-cells in live tumor slices revealed that CD49a enhances T-cell motility, especially in close proximity to tumor cells, suggesting that it may interfere with T-cell recognition of tumor cells by distracting them from productive engagement. Together, our results illuminate a new mechanism of CD8 TIL dysfunction that is induced by and dependent upon antigen-independent aspects of the TME.

It has been previously shown that CD49b is expressed on only a subset of specific effector CD8 T-cells in mouse models of arthritis and influenza or LCMV infection (18,21,27), and our work extends this observation to immunization with antigen in adjuvant. Thus, it is likely that a second signal or a specifically preprogrammed naïve T-cell subset is responsible for the initial upregulation of CD49b. However, we also showed that expression is maintained by elements in immunized mice and in the TME of BRPKp110, but not B16-F1 tumors. The B16-F1 TME may either lack these maintenance elements, or they may be antagonized by additional suppressive elements, such as TGFβ, which downregulated CD49b on activated OT-I cells *in vitro*. Surprisingly, CD49b was maintained fully on OT-I cells in the spleens of B16-OVA tumor bearing mice, and to a lesser extent on OT-I TIL, although this level was still higher than on TIL from B16-F1 tumors. We interpret this to suggest that TCR stimulation can also promote the expression of CD49b in both spleens and tumors of mice bearing B16-OVA, but continual stimulation or environmental factors in the TME ultimately lead to diminished expression. Future experiments will directly address which elements of the tumor lysate are responsible for CD49b maintenance or downregulation on CD8 T-cells.

Our results also establish that CD49a is upregulated on CD8 T-cells by elements in the TME that are present in both BRPKp110 and B16 tumors and in the splenic

environment of immunized but not naïve mice. Others have observed CD49a expression on influenza-specific T-cells after localization in airways and lungs, and also on T_{RM} T-cells, but not circulating memory T-cells (18,29,30). Together this suggests that peripheral tissue microenvironments contain element(s) that upregulate CD49a, such as TGFβ, IL-2, IL-7, or IL-15, which can upregulate CD49a directly (31,46–48). However, TGFβ does not play a significant role in controlling expression of CD49a on CD8 T-cells in BRPKp110 tumors. Future experiments will directly address which elements of the tumor lysate are responsible for CD49a upregulation or maintenance on CD8 T-cells.

We observed that expression of CD69 on CD49b SP cells was tightly associated with TCR signaling, but its expression on CD49a$^+$ cells was entirely independent, and indeed, there was little evident TCR signaling in this population. Antigen-independent expression of CD69, together with PD-1, are cardinal markers of T_{RM} cells (41), and others have shown that the environment plays a role in the generation of T_{RM} cells in the skin, pointing to an antigen-independent regulation of CD49a (49,50). The overall upregulation of CD49a, CD69, and PD-1 could thus also be explained by a differentiation of CD49a$^+$ CD8 TIL towards a T_{RM}-like phenotype.

The selective lack of TCR signaling evident in CD49a SP cells in the TME of BRPKp110 tumors was particularly striking, in that signaling was not restored by blockade of inhibitory pathways, and these cells were fully TCR responsive *in vitro*. This strongly suggested that CD49a SP cells are not making productive contacts with antigen-expressing cells. While we hypothesized that CD49a binding to collagens would trap T-cells in dense stromal areas well-separated from tumor cells, our tumor slice imaging showed that CD49a promotes increased motility, specifically in those T-cell residing in close proximity to tumor cells. Consistent with this, CD49a binding to collagen increases motility of T-cells *in vitro* and in lung tissue (25,26). Our imaging does not show clear motility of cells along ordered collagen bundles visualized by SHG. However, antibody staining of tumor sections for collagen type IV and type I, and work performed by others, demonstrates that SHG does not enable visualization of less well-ordered collagen(48). In addition, CD49a binds predominantly collagen type IV but also collagen type I (18,20). Together with the lack of TCR signaling, these data suggest that by driving motility, CD49a engagement distracts T-cells from productive engagement with tumor cells. This points to an intriguing role for CD49a in T-cell retention, not by "trapping" the cells in collagen structures but by promoting cells to rapidly move along collagen fibers, scanning the whole tissue. This role of CD49a may be especially important in T_{RM} T-cells, as their function is to remain in the tissue long-term, while scanning the tissue for re-exposure (30,52,53). However, in tumors, this mechanism may distract the T-cells from engaging effectively with their antigen and thus point to a new mechanism of immune evasion. This suggests that CD49a blockade may be an important therapeutic strategy to ensure that T-cells in tumors are able to engage with and eradicate tumors cells efficiently when co-administered with agents that overcome immune suppression in the TME.

ACKNOWLEDGEMENTS

REFERENCES

1. Erdag G, Schaefer JT, Smolkin ME, Deacon DH, Shea SM, Dengel LT, et al. Immunotype and immunohistologic characteristics of tumor-infiltrating immune cells are associated with clinical outcome in metastatic melanoma. Cancer Res. 2012;72:1070–80.
2. Aaltomaa S, Lipponen P, Eskelinen M, Kosma V-M, Marin S, Alhava E, et al. Lymphocyte infiltrates as a prognostic variable in female breast cancer. Eur J Cancer. 1992;28:859–64.
3. Liu S, Lachapelle J, Leung S, Gao D, Foulkes WD, Nielsen TO. CD8+ lymphocyte infiltration is an independent favorable prognostic indicator in basal-like breast cancer. Breast Cancer Res. 2012;14:R48.
4. Chen DS, Mellman I. Oncology Meets Immunology: The Cancer-Immunity Cycle. Immunity. Elsevier; 2013;39:1–10.
5. Ley K, Laudanna C, Cybulsky MI, Nourshargh S. Getting to the site of inflammation: the leukocyte adhesion cascade updated. Nat Rev Immunol. 2007;7:678–89.
6. Ferguson AR, Engelhard VH. CD8 T cells activated in distinct lymphoid organs differentially express adhesion proteins and coexpress multiple chemokine receptors. J Immunol Baltim Md 1950. 2010;184:4079–86.
7. Woods AN, Wilson AL, Srivinisan N, Zeng J, Dutta AB, Peske JD, et al. Differential expression of homing receptor ligands on tumor associated vasculature that control CD8 effector T cell entry. Cancer Immunol Res [Internet]. 2017 [cited 2020 Feb 24]; Available from: https://cancerimmunolres.aacrjournals.org/content/early/2017/11/01/2326-6066.cir-17-0190
8. Matheu MP, Teijaro JR, Walsh KB, Greenberg ML, Marsolais D, Parker I, et al. Three Phases of CD8 T Cell Response in the Lung Following H1N1 Influenza Infection and Sphingosine 1 Phosphate Agonist Therapy. von Herrath MG, editor. PLoS ONE. 2013;8:e58033.
9. Honda T, Egen JG, Lämmermann T, Kastenmüller W, Torabi-Parizi P, Germain RN. Tuning of Antigen Sensitivity by T Cell Receptor-Dependent Negative Feedback Controls T Cell Effector Function in Inflamed Tissues. Immunity. 2014;40:235–47.
10. Benechet AP, Menon M, Khanna KM. Visualizing T Cell Migration in situ. Front Immunol [Internet]. Frontiers; 2014 [cited 2020 Mar 30];5. Available from: https://www.frontiersin.org/articles/10.3389/fimmu.2014.00363/full
11. Espinosa-Carrasco G, Le Saout C, Fontanaud P, Michau A, Mollard P, Hernandez J, et al. Integrin β1 Optimizes Diabetogenic T Cell Migration and Function in the Pancreas. Front Immunol [Internet]. Frontiers; 2018 [cited 2020 Mar 30];9. Available from: https://www.frontiersin.org/articles/10.3389/fimmu.2018.01156/full
12. Debes GF, Arnold CN, Young AJ, Krautwald S, Lipp M, Hay JB, et al. Chemokine receptor CCR7 required for T lymphocyte exit from peripheral tissues. Nat Immunol. Nature Publishing Group; 2005;6:889–94.
13. Brown MN, Fintushel SR, Lee MH, Jennrich S, Geherin SA, Hay JB, et al. Chemoattractant receptors and lymphocyte egress from extralymphoid tissue: changing requirements during the course of inflammation. J Immunol Baltim Md 1950. 2010;185:4873–82.
14. Torcellan T, Hampton HR, Bailey J, Tomura M, Brink R, Chtanova T. In vivo photolabeling of tumor-infiltrating cells reveals highly regulated egress of T-cell subsets from tumors. Proc Natl Acad Sci. 2017;201618446.

15. Steele MM, Churchill MJ, Breazeale AP, Lane RS, Nelson NA, Lund AW. Quantifying Leukocyte Egress via Lymphatic Vessels from Murine Skin and Tumors. J Vis Exp JoVE. 2019;

16. Salmon H, Franciszkiewicz K, Damotte D, Dieu-Nosjean M-C, Validire P, Trautmann A, et al. Matrix architecture defines the preferential localization and migration of T cells into the stroma of human lung tumors. J Clin Invest. American Society for Clinical Investigation; 2012;122:899–910.

17. Bougherara H, Mansuet-Lupo A, Alifano M, Ngô C, Damotte D, Le Frère-Belda M-A, et al. Real-Time Imaging of Resident T Cells in Human Lung and Ovarian Carcinomas Reveals How Different Tumor Microenvironments Control T Lymphocyte Migration. Front Immunol [Internet]. Frontiers; 2015 [cited 2020 May 1];6. Available from: https://www.frontiersin.org/articles/10.3389/fimmu.2015.00500/full

18. Richter M, Ray SJ, Chapman TJ, Austin SJ, Rebhahn J, Mosmann TR, et al. Collagen distribution and expression of collagen-binding alpha1beta1 (VLA-1) and alpha2beta1 (VLA-2) integrins on CD4 and CD8 T cells during influenza infection. J Immunol Baltim Md 1950. 2007;178:4506–16.

19. Goldman R, Harvey J, Hogg N. VLA-2 is the integrin used as a collagen receptor by leukocytes. Eur J Immunol. 1992;22:1109–14.

20. Hemler ME. VLA Proteins in the Integrin Family: Structures, Functions, and Their Role on Leukocytes. Annu Rev Immunol. 1990;8:365–400.

21. Fougerolles AR de, Sprague AG, Nickerson-Nutter CL, Chi-Rosso G, Rennert PD, Gardner H, et al. Regulation of inflammation by collagen-binding integrins α1β1 and α2β1 in models of hypersensitivity and arthritis. J Clin Invest. American Society for Clinical Investigation; 2000;105:721–9.

22. Meharra EJ, Schön M, Hassett D, Parker C, Havran W, Gardner H. Reduced gut intraepithelial lymphocytes in VLA1 null mice. Cell Immunol. 2000;201:1–5.

23. Sandoval F, Terme M, Nizard M, Badoual C, Bureau M-F, Freyburger L, et al. Mucosal Imprinting of Vaccine-Induced CD8+ T Cells Is Crucial to Inhibit the Growth of Mucosal Tumors. Sci Transl Med. American Association for the Advancement of Science; 2013;5:172ra20-172ra20.

24. Richter MV, Topham DJ. The α1β1 Integrin and TNF Receptor II Protect Airway CD8+ Effector T Cells from Apoptosis during Influenza Infection. J Immunol. American Association of Immunologists; 2007;179:5054–63.

25. Conrad C, Boyman O, Tonel G, Tun-Kyi A, Laggner U, de Fougerolles A, et al. α 1 β 1 integrin is crucial for accumulation of epidermal T cells and the development of psoriasis. Nat Med. Nature Publishing Group; 2007;13:836–42.

26. Reilly EC, Emo KL, Buckley PM, Reilly NS, Chaves FA, Yang H, et al. TRM Integrins CD103 and CD49a Differentially Support Adherence and Motility After Resolution of Influenza Virus Infection. bioRxiv. Cold Spring Harbor Laboratory; 2020;2020.02.14.947986.

27. Andreasen SØ, Thomsen AR, Koteliansky VE, Novobrantseva TI, Sprague AG, Fougerolles AR de, et al. Expression and Functional Importance of Collagen-Binding Integrins, α1β1 and α2β1, on Virus-Activated T Cells. J Immunol. American Association of Immunologists; 2003;171:2804–11.

28. Murray T, Fuertes Marraco SA, Baumgaertner P, Bordry N, Cagnon L, Donda A, et al. Very Late Antigen-1 Marks Functional Tumor-Resident CD8 T Cells and Correlates

with Survival of Melanoma Patients. Front Immunol [Internet]. 2016 [cited 2020 Feb 24];7. Available from: https://www.ncbi.nlm.nih.gov/pmc/articles/PMC5150229/

29. Topham DJ, Reilly EC. Tissue-Resident Memory CD8+ T Cells: From Phenotype to Function. Front Immunol. 2018;9:515.

30. Cheuk S, Schlums H, Gallais Sérézal I, Martini E, Chiang SC, Marquardt N, et al. CD49a Expression Defines Tissue-Resident CD8+ T Cells Poised for Cytotoxic Function in Human Skin. Immunity. 2017;46:287–300.

31. Melssen MM, Olson W, Wages NA, Capaldo BJ, Mauldin IS, Mahmutovic A, et al. Formation and phenotypic characterization of CD49a, CD49b and CD103 expressing CD8 T cell populations in human metastatic melanoma. OncoImmunology. 2018;7:e1490855.

32. Hombrink P, Helbig C, Backer RA, Piet B, Oja AE, Stark R, et al. Programs for the persistence, vigilance and control of human CD8 + lung-resident memory T cells. Nat Immunol. Nature Publishing Group; 2016;17:1467–78.

33. Zhang N, Bevan MJ. Transforming Growth Factor-β Signaling Controls the Formation and Maintenance of Gut-Resident Memory T Cells by Regulating Migration and Retention. Immunity. Elsevier; 2013;39:687–96.

34. Moran AE, Holzapfel KL, Xing Y, Cunningham NR, Maltzman JS, Punt J, et al. T cell receptor signal strength in Treg and iNKT cell development demonstrated by a novel fluorescent reporter mouse. J Exp Med. 2011;208:1279–89.

35. Allegrezza MJ, Rutkowski MR, Stephen TL, Svoronos N, Perales-Puchalt A, Nguyen JM, et al. Trametinib Drives T-cell–Dependent Control of KRAS-Mutated Tumors by Inhibiting Pathological Myelopoiesis. Cancer Res. American Association for Cancer Research; 2016;76:6253–65.

36. Hargadon KM, Brinkman CC, Sheasley-O'Neill SL, Nichols LA, Bullock TNJ, Engelhard VH. Incomplete Differentiation of Antigen-Specific CD8 T Cells in Tumor-Draining Lymph Nodes. J Immunol. American Association of Immunologists; 2006;177:6081–90.

37. Salerno EP, Olson WC, McSkimming C, Shea S, Slingluff Jr. CL. T cells in the human metastatic melanoma microenvironment express site-specific homing receptors and retention integrins. Int J Cancer. 2014;134:563–74.

38. Rosean CB, Bostic RR, Ferey JCM, Feng T-Y, Azar FN, Tung KS, et al. Preexisting Commensal Dysbiosis Is a Host-Intrinsic Regulator of Tissue Inflammation and Tumor Cell Dissemination in Hormone Receptor–Positive Breast Cancer. Cancer Res. American Association for Cancer Research; 2019;79:3662–75.

39. Hashimoto M, Kamphorst AO, Im SJ, Kissick HT, Pillai RN, Ramalingam SS, et al. CD8 T Cell Exhaustion in Chronic Infection and Cancer: Opportunities for Interventions. Annu Rev Med. Annual Reviews; 2018;69:301–18.

40. Jiang X, Clark RA, Liu L, Wagers AJ, Fuhlbrigge RC, Kupper TS. Skin infection generates non-migratory memory CD8 + T RM cells providing global skin immunity. Nature. Nature Publishing Group; 2012;483:227–31.

41. Kumar BV, Ma W, Miron M, Granot T, Guyer RS, Carpenter DJ, et al. Human tissue-resident memory T cells are defined by core transcriptional and functional signatures in lymphoid and mucosal sites. Cell Rep. 2017;20:2921–34.

42. Chen X, Nadiarynkh O, Plotnikov S, Campagnola PJ. Second harmonic generation microscopy for quantitative analysis of collagen fibrillar structure. Nat Protoc.

2012;7:654–69.

43. Mostaço-Guidolin L, Rosin NL, Hackett T-L. Imaging Collagen in Scar Tissue: Developments in Second Harmonic Generation Microscopy for Biomedical Applications. Int J Mol Sci [Internet]. 2017 [cited 2020 Apr 20];18. Available from: https://www.ncbi.nlm.nih.gov/pmc/articles/PMC5578161/

44. Dustin ML, Bromley SK, Kan Z, Peterson DA, Unanue ER. Antigen receptor engagement delivers a stop signal to migrating T lymphocytes. Proc Natl Acad Sci. 1997;94:3909–13.

45. Friedman RS, Jacobelli J, Krummel MF. Mechanisms of T cell motility and arrest: Deciphering the relationship between intra- and extracellular determinants. Semin Immunol. 2005;17:387–99.

46. Gao Y, Souza-Fonseca-Guimaraes F, Bald T, Ng SS, Young A, Ngiow SF, et al. Tumor immunoevasion by the conversion of effector NK cells into type 1 innate lymphoid cells. Nat Immunol. 2017;18:1004–15.

47. Rubio MA, Sotillos M, Jochems G, Alvarez V, Corbií AL. Monocyte activation: rapid induction of α1/β1 (VLA-1) integrin expression by lipopolysaccharide and interferon-γ. Eur J Immunol. 1995;25:2701–5.

48. Ni X, Fu B, Zhang J, Sun R, Tian Z, Wei H. Cytokine-Based Generation of CD49a+Eomes−/+ Natural Killer Cell Subsets. Front Immunol [Internet]. 2018 [cited 2020 Feb 25];9. Available from: https://www.frontiersin.org/articles/10.3389/fimmu.2018.02126/full

49. Mackay LK, Rahimpour A, Ma JZ, Collins N, Stock AT, Hafon M-L, et al. The developmental pathway for CD103 + CD8 + tissue-resident memory T cells of skin. Nat Immunol. Nature Publishing Group; 2013;14:1294–301.

50. Adachi T, Kobayashi T, Sugihara E, Yamada T, Ikuta K, Pittaluga S, et al. Hair follicle-derived IL-7 and IL-15 mediate skin-resident memory T cell homeostasis and lymphoma. Nat Med. 2015;21:1272–9.

51. Pena A-M, Boulesteix T, Dartigalongue T, Schanne-Klein M-C. Chiroptical Effects in the Second Harmonic Signal of Collagens I and IV. J Am Chem Soc. American Chemical Society; 2005;127:10314–22.

52. Ariotti S, Hogenbirk MA, Dijkgraaf FE, Visser LL, Hoekstra ME, Song J-Y, et al. Skin-resident memory CD8+ T cells trigger a state of tissue-wide pathogen alert. Science. American Association for the Advancement of Science; 2014;346:101–5.

53. Masopust D, Soerens AG. Tissue-Resident T Cells and Other Resident Leukocytes. Annu Rev Immunol. 2019;37:521–46.
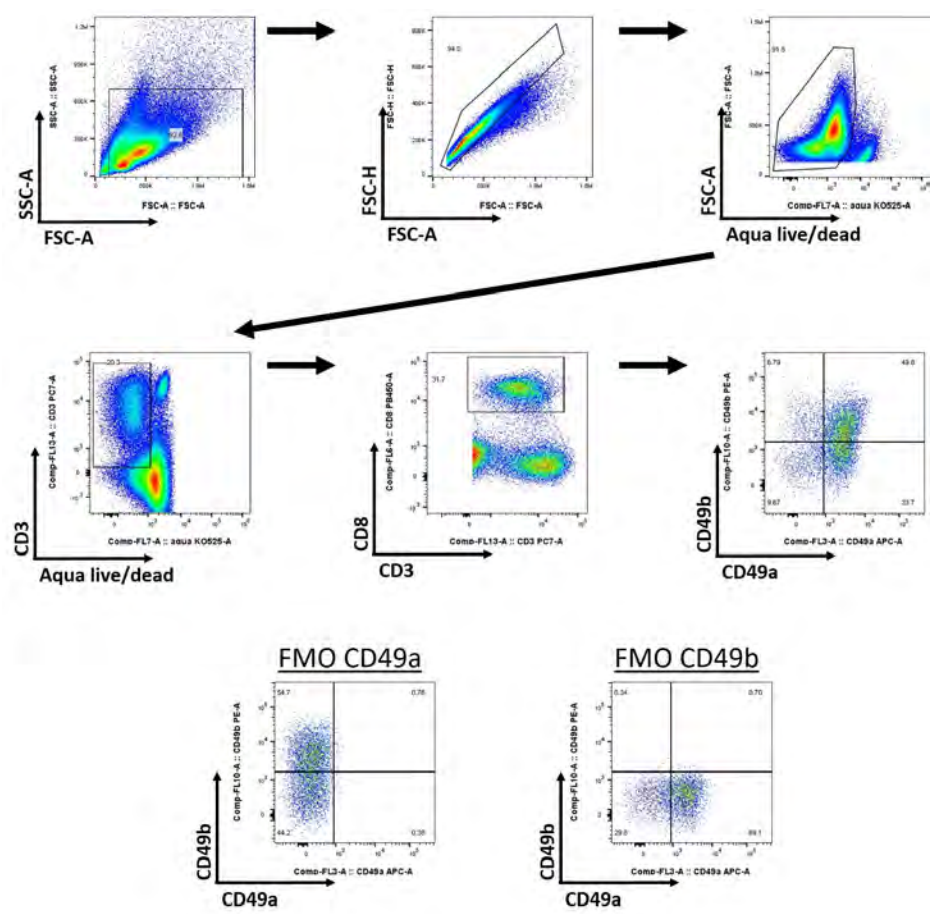
Supplemental Figure 1. Gating strategy for flow cytometry experiments. Debris, doublets and dead cells were excluded (top panels), CD3+ and CD8+ T cells were selected and CD49a and CD49b positivity was determined based on their respective fluorescence minus one (FMO) control samples.
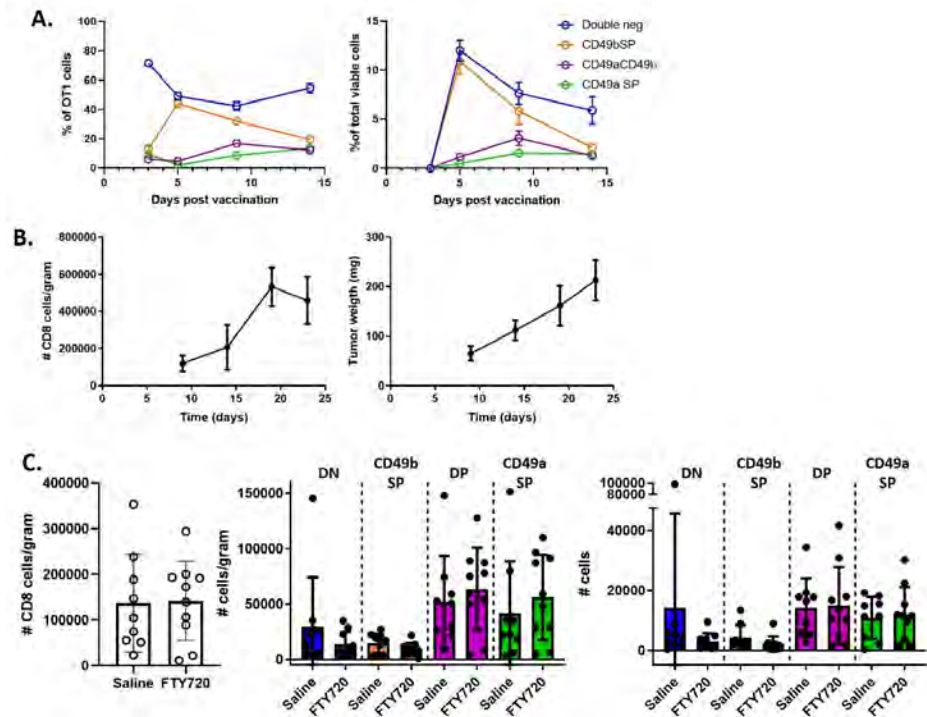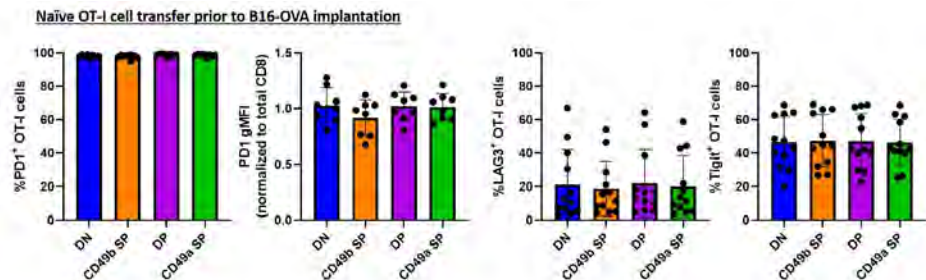
Supplemental Figure 2. (A) 5x10^6 Thy1.1$^+$ OT-I splenocytes were transferred IV into C57BL/6 mice. 1 day post transfer, mice were vaccinated IV with ovalbumin, polyIC and anti-CD40. Spleens of vaccinated mice were harvested 3, 5, 9 and 14 days post vaccination and analyzed for CD49a and CD49b expression on Thy1.1$^+$ CD3$^+$ CD8$^+$ cells by flow cytometry. (B) C57BL/6 mice were implanted SC with BRPKp110 breast carcinoma tumors. Tumors were harvested on day 9, 14, 19 or 23 (as indicated), single cell suspensions were prepared and enriched for CD45$^+$ cells. CD3$^+$CD8$^+$ cells/gram of tumor were quantified with flow cytometry. (C) C57BL/6 mice were implanted SC with BRPKp110 breast carcinoma tumors. Baseline tumors were harvested on day 14 and processed for flow cytometry as in (B). Other BRPKp110-bearing animals received daily IP injections with FTY720 or saline control. Treated tumors were harvested on day 23 and processed for flow cytometry.
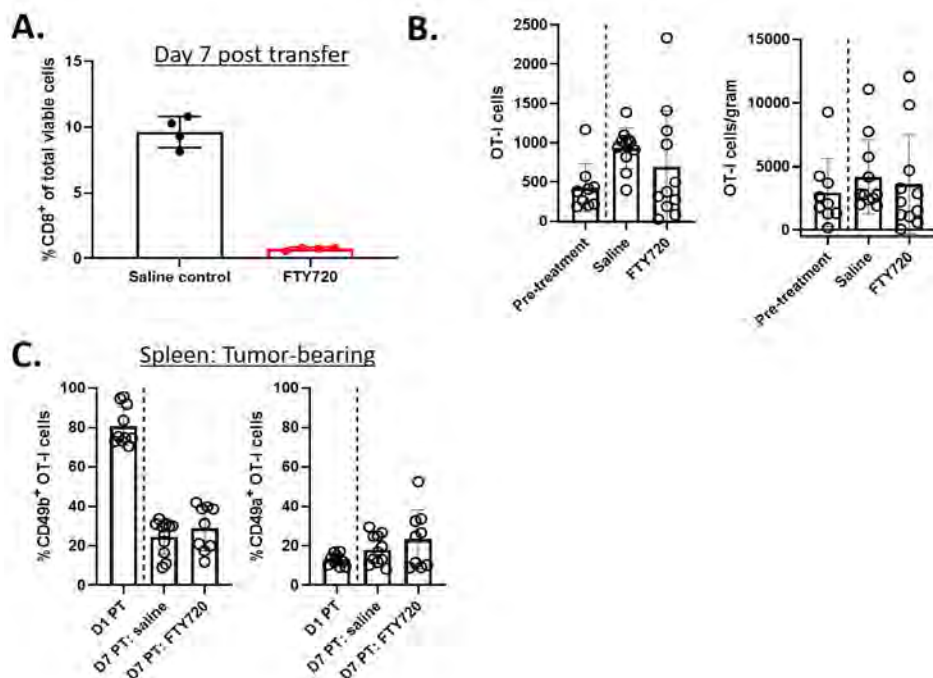
Supplemental Figure 3. (A/B) 5x10^6 Thy1.1$^+$ OT-I splenocytes were transferred IV into C57BL/6 mice. 1 day post transfer, mice were vaccinated IV with ovalbumin, polyIC and anti-CD40. 5 days post vaccination splenocytes were depleted for CD49a$^+$ cells and subsequently enriched for CD49b$^+$ cells. Enriched cells were evaluated for Thy1.1$^+$ fraction to ensure adoptive transfer of 1x10^6 CD49b SP Thy1.1$^+$ OT-I effectors. Cells were transferred IV into BRPKp110 tumor-bearing-mice. Baseline tumors were harvested on day 1 post transfer and processed for flow cytometry. Other animals received daily IP injections with FTY720 or saline control and blood samples and tumors were harvested on day 7 post transfer. (A) Blood samples were analyzed for CD3$^+$ CD8$^+$ cells by flow cytometry. (B) Tumor were processed into single-cell suspensions, enriched for CD45$^+$ and analyzed for CD49b and CD49a expression on Thy1.1$^+$ CD3$^+$ CD8$^+$ cells. (C) Spleens were processed into single-cell suspensions and analyzed for CD49b and CD49a expression on Thy1.1$^+$ CD3$^+$ CD8$^+$ cells.
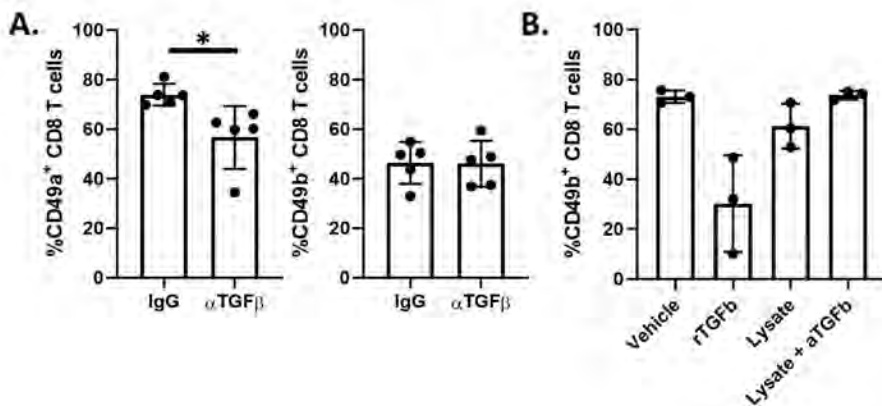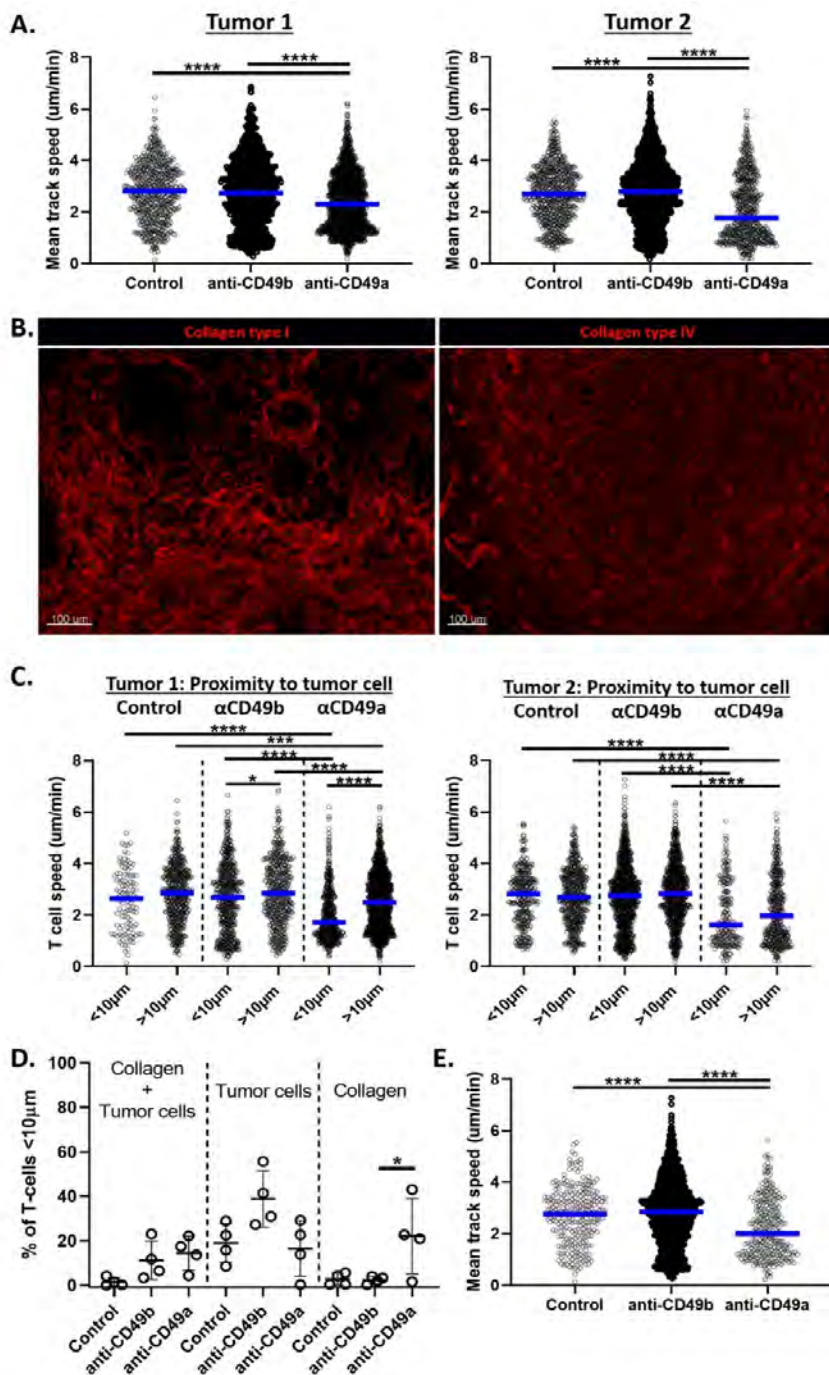
Supplemental Figure 4. (A) C57BL/6 mice were implanted SC with BRPKp110 breast carcinoma tumors. Mice were injected IP with anti-TGFβ1/2/3 or IgG control every 3 days between day 8-19 post tumor implantation. Tumors were harvested and single-cell suspensions were enriched for $CD45^+$ cells. CD45 fractions were analyzed for CD49a and CD49b expression on $CD3^+$ $CD8^+$ cells. **(B)** $Thy1.1^+$ OT-I splenocytes were enriched for $CD8^+$ cells by magnetic bead enrichment. Cells were activated for 48 hours with CD3/CD28 activation beads and cultured for an additional 3 days in presence of IL-2 and IL-7. Next, OT-I cells were cultured for 24 hours with recombinant human TGFβ1, BRPKp110-derived tumor lysate or lysate with anti-TGFβ blocking antibodies. Cells evaluated for CD49b expression by flow cytometry.

Supplemental Figure 5. $5x10^6$ $Thy1.1^+$ OT-I splenocytes were transferred IV into C57BL/6 mice. 1 day post transfer, mice were subcutaneously injected with B16-OVA tumor cells. Tumors were harvested on day 19 and processed for flow cytometry evaluation.
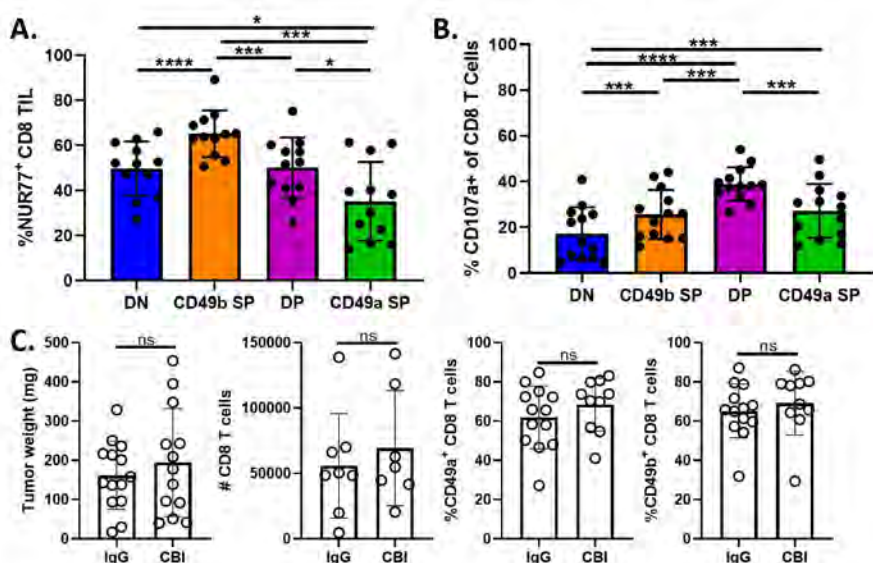
Supplemental Figure 6. (A) Nur77-GFP reporter mice were implanted SC with BRPKp110 breast carcinoma. Tumors were harvested on day 14, single cell suspensions were prepared and enriched for CD45$^+$ cells. CD45 fraction was analyzed for Nur77-GFP, CD49a and CD49b expression on CD3$^+$ CD8$^+$ cells. (B) C57BL/6 mice were implanted SC with BRPKp110 breast carcinoma. Tumors were harvested on day 14, single cell suspensions were prepared and enriched for CD8$^+$ cells. Cells were cultured with CD3/CD28 stimulation beads for 4-6 hours in presence of Brefeldin A and CD107a antibody. Cells were analyzed for expression CD49a, CD49b and CD107a expression on CD3$^+$ CD8$^+$ cells with intracellular staining for flow cytometry. (C) Nur77-GFP reporter mice were implanted SC with BRPKp110 breast carcinoma. Mice were IP injected 48 hours prior to harvest with a checkpoint blockade inhibitor (CBI) cocktail including anti-PD1, anti-LAG3 and anti-TIM3. Tumors were harvested, single-cell suspensions were prepared and enriched for CD45$^+$ cells. CD45 fraction was analyzed for CD49a and CD49b expression on CD3$^+$ CD8$^+$ cells by flow cytometry.

Supplemental Figure 7. CD2-dsRed mice were implanted SC with BRPKp110-GFP tumors. Tumors were harvested on day 21/22, embedded in agarose and cut into thick slices of

approximately 100-200μicrons. Slices were incubated with anti-CD49a or anti-CD49b blocking antibodies for 2 hours and assessed for CD2$^+$ T-cells, GFP$^+$ BRPKp110 cells and collagen fibers with second harmonics generation (SHG) on a 2-photon microscope. 30-minute videos of 2 fields per slice were made while maintaining oxygenation and 37°C with warm flowing media. (A) Mean track speed of the CD2$^+$ T-cells in each tumor evaluated. Treatment groups were compared with an ordinary one-way ANOVA and Tukey's multiple comparisons test. (B) C57BL/6 mice were implanted with BRPKp110 tumors. Day 21 tumors were harvested, fixed and thin sections were cut and stained with collagen type I or collagen type IV antibodies. (C) Mean track speed of the CD2$^+$ T-cells, stratified by distance to GFP$^+$ BRPKp110 tumor cells for tumor 1 (left) and tumor 2 (right). Close proximity: <10μm, large distance: >10μm. Groups were compared with an ordinary one-way ANOVA and Tukey's multiple comparisons test. (D) Live tumor slices were prepared and imaged by 2-photon microscopy as described in (A). Fraction of CD2$^+$ T-cells are displayed per field: fraction of cells <10μm to closest GFP$^+$ BRPKp110 tumor cell, <10μm to closest SHG-collagen fiber or <10μm to tumor cell and collagen (left). (E) Mean track speed of those CD2$^+$ T-cells located <10μm to tumor cells and >10μm from SHG-collagen.